AN EXPERIMENTAL STUDY ON THE INTERACTION OF COAXIAL AND CO-ROTATING VORTEX RINGS

By

Jagannadha Reddy Satti

RECOMMENDED: Chuen-Yen Lin

Debendra K Das

Jifeng Peng

Advisory Committee Chair

Joseph Lee

Chair, Department of Mechanical Engineering

APPROVED: Gary Acho

Dean, College of Engineering and Mines

Laurence K Duffy

Dean of the Graduate School

Jan 31, 2012

Date

AN EXPERIMENTAL STUDY ON THE INTERACTION OF COAXIAL AND CO-ROTATING VORTEX RINGS

A

THESIS

Presented to Faculty

of the University of Alaska Fairbanks

in Partial Fulfillment of the Requirements

for the Degree of

MASTER OF SCIENCE

By

JAGANNADHA REDDY SATTI, B.Tech

Fairbanks, Alaska

May 2012

Abstract

The study investigated the role of formation time, Reynolds Number, and non-dimensional frequency number, the three most significant parameters in the dynamics of vortex rings, in the interaction between co-axial and co-rotating vortex rings and in the ring behaviors of merging and leapfrogging. To generate and investigate vortex rings with the required characteristics, two laminar vortex rings were generated consecutively from a piston–cylinder apparatus such that the rings propagated in the same direction and that the spatial separation between them decreased until they began merging. Using digital particle image velocimetry to measure the flow fields as well as the trajectory and circulation of the individual rings, a series of experiments were conducted at three formation times, with the experiments at each formation time repeated at different Reynolds Numbers, and the experiments at each Reynolds Number in turn repeated at different non-dimensional frequency numbers. The results indicate that at low Reynolds Numbers, the total circulation in the flow is relatively constant before and after the rings merge. However, at high Reynolds Numbers, the total circulation begins rapidly decreasing upon the contact of two vortex ring cores, indicating a transition to a turbulent vortex ring during merging, before stabilizing at a lower level, indicating that the merged ring has transitioned back to a laminar vortex ring after shedding some circulation.

Table of Contents

Page

Page

Page

Page

List of Figures

Page

Page

Page

Page

Page

Acknowledgments

First and foremost, I want to thank my principal advisor, Dr. Jifeng Peng, for whom I had the honor of being his first graduate student. I appreciate all that he has taught me regarding the importance of experimental fluid mechanics and his contribution of time and ideas in making my experience productive and stimulating. I would also like to thank my advisory committee members, Dr. Debendra K. Das and Dr. Chuen-Sen Lin. I greatly appreciate the financial support from the mechanical engineering department that allowed me to complete this thesis, and am thankful for Erick Johnson's help in machining the parts required for the experimental setup.

Last but not least, I remain forever grateful to my parents, Mr. Prabhakara Reddy Satti and Mrs. Parvathi, and my sister, Ms. Raja Rajeswari, on whose constant encouragement and love I have relied throughout my entire university experience.

Chapter 1 General Introduction

1.1 Introduction

Vortex rings are commonly occurring natural phenomena that result from sudden changes in fluid flow. While generally not visible to the naked eye, vortex rings that arise from the occurrence of certain extreme phenomena may be visible. These phenomena include volcanic eruptions and atomic bomb explosions, during which the sudden ejection of hot gases forms an outer boundary that assumes an observable ring-like structure, such as that of a smoke ring.

Over a century of research into vortex rings has demonstrated that certain animals, including birds, fish, squids, and dolphins, use vortex rings for propulsion. Among the aquatic species that have been found to produce vortex rings, several have been observed to produce these rings in a sequence at their fins (Rayner 1979 (a)). A study of the sequenced production of vortex rings produced by underwater animals demonstrated that such vortex rings produced in sequence increase propulsion efficiency (Dabiri and Gharib 2005). In a like manner, birds produce vortex rings at their wing tips to produce lift (Rayner 1979 (b)). Recently, it was discovered that the human heart also produces vortex rings in the diastole stroke of the heart to improve the mixing of blood inside the heart. As the production of the rings has been observed to vary with the health of the heart, the nature of this vortex ring formation inside the heart may be an important indicator of heart health (Gharib et al. 2006).

1.1 Present work

The study of vortex rings is multifaceted and encompasses research into their motion, stability, and interactions. Due to their complexity, complete understanding of vortex rings has yet to be attained, even after more than a century of research. The goal of this study was to contribute to this understanding by observing and evaluating the dynamics of vortex ring interactions using digital particle image velocimetry (DPIV) to perform quantitative analysis of the interaction between a coaxial and a co-rotating vortex ring.

1.2 Organization

Chapter 1 provides a general introduction to vortex rings and the subject investigated in this work. Chapter 2 provides background information on the production of vortex rings and the parameters that play an important role in their interactions. Chapter 3 describes the methodology, experimental setup, and DPIV technique used to perform the experiments. Chapter 4 provides a complete and detailed analysis of the results of the experiments, chapter 5 summarizes the major findings and the conclusions derived from their analysis.

Chapter 2 Background and Theory

2.1 Vortex rings

The most recent definition of a vortex ring is provided by Lim, who defined the phenomenon as "a bounded region of vorticity in which the vortex lines form closed loops" (Lim and Nickels 1995). These closed vortex loops, which have been observed to assume a primarily circular shape and propagate forward to transport extra fluid within them into a surrounding medium, are formed by the rolling up of vortex sheets at the edge of a nozzle as a finite column of liquid is ejected. After the vortex layers of fluid are ejected from the nozzle and start rolling up, the rolling vortex sheet forms a closed-loop vortex line—the vortex ring (Batchelor 1967). The formation of vortex rings varies with different L/D ratios, where L is the column (stroke) length and D is the diameter of nozzle (Weigand and Gharib 1997). Understanding the structure of a vortex ring requires identification of two critical parameters, vorticity and circulation. During the formation of a vortex ring, the circulation increases until the surrounding fluid stops entraining into the ring, at which point the circulation becomes constant (Lim and Nickels 1995).

2.1.1 Vorticity

A measure of fluid rotation, vorticity is a vector quantity whose direction is determined by the direction of the rotation. When a fluid is rotated in a plane, it moves in a direction normal to the plane of rotation: toward the outward normal if rotated counterclockwise or toward the inward normal if rotated clockwise. As shown in Figure 2.1, a counterclockwise rotating vortex tends to move fluid in the $\hat{k}$ direction on the XY (horizontal) plane, in the $\hat{\imath}$ direction on the YZ plane, and in the $\hat{\jmath}$ direction in the ZX plane (Kundu and Cohen 2004). Thus, vorticity has three components whose relationship can be mathematically expressed as the following:

$$\vec{\nabla}\times\vec{V} = \hat{\imath}\xi + \hat{\jmath}\eta + \hat{k}\varsigma \tag{1}$$

where $\xi = \frac{\partial w}{\partial y} - \frac{\partial v}{\partial z}$; $\eta = \frac{\partial u}{\partial z} - \frac{\partial w}{\partial x}$; $\varsigma = \frac{\partial v}{\partial x} - \frac{\partial u}{\partial y}$

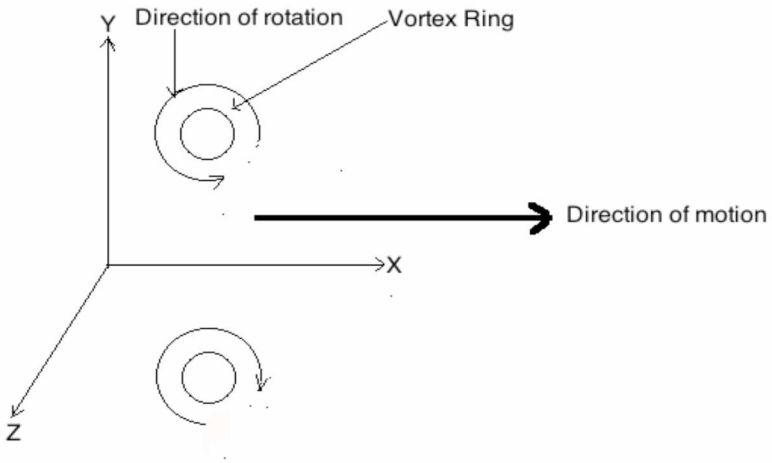

Figure 2.1 Illustration of vortex ring in planes

2.1.2 Circulation

Mathematically, circulation is defined as a line integral of the velocity vector around a closed path, around which the circulation is measured (Kundu and Cohen 2004). As the term circulation in this context refers to the circulation of a velocity vector, circulation around a closed path in this study was determined using the following formula:

$$C = \oint \vec{V} . \overrightarrow{dl} \tag{2}$$

2.2 Characterization of vortex rings

Among the numerous methods that have been used to characterize vortex rings, those that use several non-dimensional factors have been found to provide a reasonable characterization. In the dynamics and interaction between a coaxial and a co-rotating vortex ring, the non-dimensional factors of formation time, Reynolds Number, and non-dimensional frequency have been found to play important roles.

2.2.1 Formation time

Most recent work concerning the formation of vortex rings has stemmed from the work of Gharib. Based on the results of a study using cylindrical piston geometry to perform vortex generation to determine the largest circulation that a vortex ring can attain at a constant piston speed, they defined formation time as the ratio of stroke length to the diameter of the nozzle (Gharib et al. 1998):

$$L = \int_0^t u_p(t)dt \tag{3}$$

$$U_p = \left(\frac{1}{t\int_0^t u_p\, dt}\right) \tag{4}$$

$$\frac{L}{D} = \frac{U_p\, t}{D} = Formation\ time \tag{5}$$

Having found that for simple configurations, fixed piston speed allows only for variation of the stroke length L_0, as well as that circulation was maximized for $L_0/D_0 = 4$, they

referred to the maximum attainable value of L_0/D_0 as the formation number (Weigand and Gharib 1997; Dabiri and Gharib 2004).

2.2.2 Reynolds Number

Defined as the ratio of inertia force to viscous force, the Reynolds Number (Re) is a dimensionless parameter important in the study of viscous fluids. The original Reynolds Number ratio can be modified for application to the study of vortex rings. For experimental calculations using a cylinder and nozzle, the Reynolds Number can be calculated using the traditional pipe flow formulation, where U is the velocity inside the cylinder, D is the diameter of the nozzle, and ν is the kinematic viscosity:

$$Re = \frac{UD}{\nu} \tag{6}$$

Although the Reynolds Number can also be determined directly from the vortex ring, the formula used to do so cannot be universally defined, as it depends on the parameters of velocity and length. One method of determining Reynolds Number that is derived from vortex ring circulation (Glezer 1988) requires relatively complex measurement of the fluid flow field and integration of the vorticity field. However, this method may be simplified with the use of Stokes' theorem, as shown in equation (7) (Kundu and Cohen 2004), in which the velocity field U is integrated onto surface S bounded by line l.

$$Re = \frac{\Gamma}{\upsilon} \tag{7}$$

$$\Gamma = \int_S \nabla X\, u.dS = \oint_l u.dl \tag{8}$$

2.2.3 Non-dimensional frequency number

A pulsed jet can be used to produce multiple vortex rings at different time intervals. Non-dimensional frequency number (SR_L), one parameter by which a pulsed jet can be defined, can be calculated using the following formula:

$$SR_L = f\,L/U_J \tag{9}$$

$$U_J = L/t_p \tag{10}$$

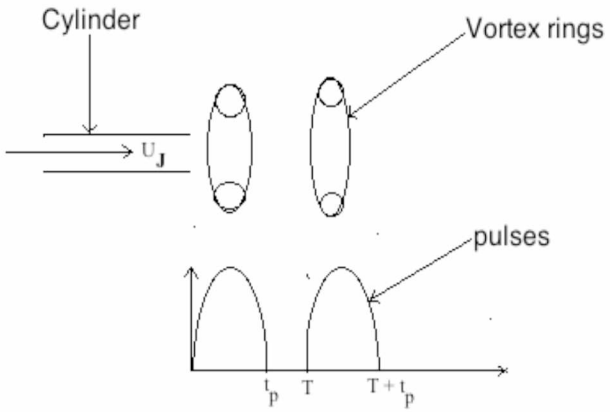

Figure 2.2 Non-dimensional frequency curves of vortex rings

Where U_J is the time-average velocity of the piston, L is the length of the piston traveled, f is the frequency, t_p is the pulse time of the piston, and T is the sum of the pulse time of the piston and the time gap between the pulses. From this formula is derived the formula used to determine the separation of pulses, $SR_L = t_p / T$, which can have a value between 0 and 1 (Krueger and Gharib 2005). Non-dimensional frequency curves of vortex rings different vortex ring pulses are shown in Figure 2.2.

2.3 Evolution of vortex rings

Wide research using a variety of numerical, analytical, and experimental approaches has revealed that the evolution of a vortex ring consists of three stages: the formation stage, the laminar or turbulent stage, and the decay stage. During the formation stage, the vortex ring starts forming when the vortex layers inside the cylinder emerge from the nozzle and start rolling up to form a closed loop of vortex line, thus producing a vortex ring. This ring entrains surrounding fluid into it, resulting in an increase in the circulation of the ring that is clearly measurable during this stage. The circulation continues increasing to a particular point, depending on the initial conditions, and is identified as laminar or turbulent, depending on its circulation level.

Laminar rings do not experience any sudden decrease in circulation after the formation stage. In contrast, during the laminar or turbulent stage, turbulent rings experience a sudden decrease in circulation to a constant level, which they maintain for some time before beginning to decay during the decay stage. At this stage, the ring starts

to lose circulation rapidly until ultimately disappearing into the surrounding fluid (Maxworthy 1972).

2.4 Laboratory formation of vortex rings

Production of vortex rings in the laboratory is generally achieved by ejection of fluid from either an open cylinder or an orifice, which pushes a column of fluid of cylinder length L_0 and diameter (or orifice) D_0. After the vortex layers are formed at the wall of the cylinder, they move outward when the fluid is pushed out. These vortex layers at the edge of circular outlet then start to spiral to form a toroidal structure of rotating fluid—that is, a vortex ring. The formation of the rings is shown in Figure. 2.3.

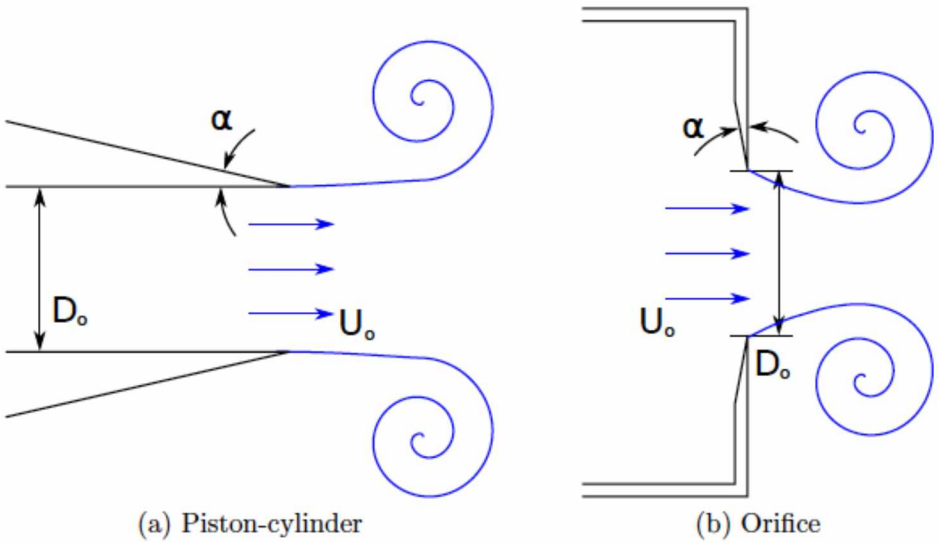

Figure 2.3 Typical vortex ring geometries (Shariff and Leonard 1992)

2.5 Slug flow model

Vortex ring formation is commonly described using the slug flow model. By assisting in the control of the initial conditions in vortex ring formation, such as circulation Γ_0 and impulse I_0, the slug flow model allows for estimation of the initial conditions of the vortex ring as a function of generation parameters. Considering boundary layer approximation and assuming that the velocity of fluid is the same at the outlet of the cylinder, the approximate rate of flux can be described using the following formula (Lim and Nickels 1995).

$$\frac{d\Gamma}{dt} = \int \omega \, udr \simeq \frac{\partial u}{\partial r} udr \simeq \int_0^{U_p(t)} \frac{\partial u2}{2\partial r} \simeq \frac{1}{2} Up2(t) \tag{11}$$

Assuming that all vorticity formed will roll up and form a vortex ring, the initial vortex ring has an initial circulation of Γ_0, which can be described using the following formula (Krueger 2010):

$$\Gamma_0 = \int_0^{T0} \frac{1}{2} U_P^2 \mathrm{dt} \tag{12}$$

2.6 Interactions

The literature on velocity rings focuses on three types of interaction above all others, coaxial interaction between two rings moving in the same direction, coaxial interaction between rings moving in opposite directions, and interaction between two rings

interacting at an angle Φ (Lim and Nickels 1995) which are shown in Figures. 2.4, 2.5, and 2.6, respectively.

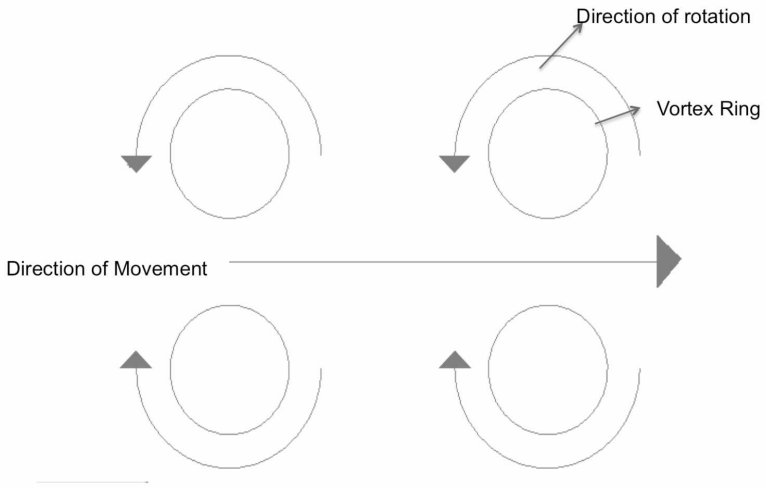

Figure 2.4 Coaxial interaction between vortex rings moving in the same direction

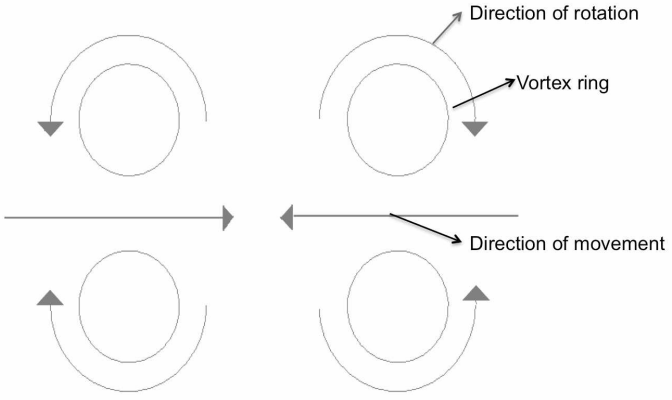

Figure 2.5 Coaxial interaction between vortex rings moving in opposite directions

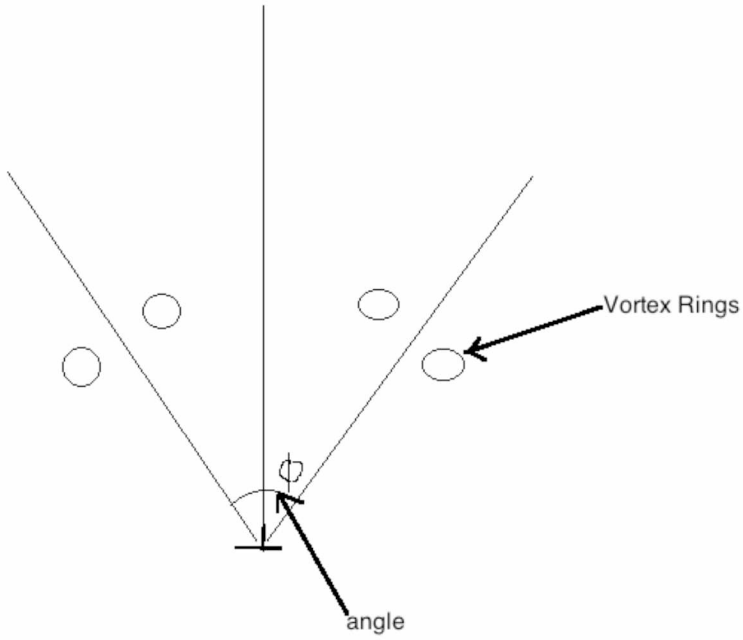

Figure 2.6 Interaction between vortex rings at a defined angle

The experiments in this study were conducted to study the dynamics of the interaction between coaxial and co-rotating vortex rings. This type allows for an interesting observation: that the rings exchange positions as they move, a phenomenon referred to as leapfrogging, which is explored in detail in Chapter 4. Research into the interaction between vortex rings began with Maxworthy's (1972) experiments on coaxial interactions, which found that two identical vortex rings merge with each other and that the velocity of the trailing ring is higher than leading ring. In similar experiments, Oshima et al. (1975) found that leapfrogging can occur only when the time gap between the rings is between 0.15 and 0.25 seconds, and observed a large increase in ring diameter at low velocities but both an increase in ring diameter and separation into smaller rings at

higher velocities. Based on his findings, Oshima proposed that leapfrogging is not a trivial phenomenon and is one that requires satisfaction of certain conditions, such a certain ring speed and diameter. Liu and Hsu (1985) observed that the number of times that rings leapfrog before merging depends on their Reynolds Number and the initial conditions that exist between them, an observation later confirmed by Oshima and Izutsu (1988) finding that leapfrogging is a function of the Reynolds' number of rings. Most of these findings were derived from experiments in which laminar vortex rings were used to study the interaction between the vortex rings.

Considering the non-dimensional time between the rings and performing experiments at different Reynolds Numbers, Lim (1997) confirmed the influence of a time gap between the rings. His results, which showed the results between the non-dimensional time and Reynolds Number, indicated that successful leapfrogging occurs between Reynolds Numbers 1000 and 2100. As such, they accord with the results of Yamada and Matsui (1978), who observed leapfrogging at high Reynolds Numbers. Lim also observed that with a sufficiently large time gap between the rings, leapfrogging can be seen at even low Reynolds Numbers. As the time gap decreases, the trailing ring has less time to develop, whereas as the time gap increases, the time delay between the rings increases, which may prevent the rings from coming together. As low Reynolds Number rings require more time to develop, they require a greater time gap between the rings. Thus, the time gap between the rings is an important parameter in determining whether leapfrogging will occur.

The few studies that have investigated the circulation of rings undergoing interaction indicate that the circulation of the vortex ring is an important parameter in the interaction between the coaxial and the co-rotating vortex ring. Among these studies, Maxworthy reported that high circulation of vortex rings promotes leapfrogging (Maxworthy 1977). Gharib et al. found that an isolated vortex ring is produced when the ratio of stroke length to the diameter of the tube, which they called the formation number, is less than four, and that a trailing jet is produced with the vortex ring when the formation number is greater than four (Gharib et al. 1998). By using a high formation number to produce two successive vortex rings, the interaction between the trailing jet of the leading vortex ring and the trailing vortex ring, which disturbs the interaction of the two vortex rings, can be observed.

Chapter 3 Methdology

3.1 Experimental setup

As discussed in chapter 2, vortex rings can be produced by many types of vortex generators. Some of these generators produce vortex rings by controlling the fluid pressure in a cylinder using a pressure-controlling valve, while others produce vortex rings using two cylinders and a motor setup. Using the latter method, the experimental setup in this study consisted of a 2 × 0.6 × 0.6 m rectangular acrylic water tank and two cylinders, one (Cylinder 1) with a diameter of 0.05 m and one (Cylinder 2) with a diameter of 0.25 m, connected by a rubber tube and with pistons of diameters equal to the inner diameter of the cylinders. The piston inside Cylinder 1 was connected to a linear actuator, a device that converts the rotary motion of a motor to linear movement. When the linear actuator moved the piston inside Cylinder 1, the pressure inside the cylinder increased, causing the water to move toward and exert force on Cylinder 2, thereby generating a vortex ring. When the linear actuator moved backward, the pressure inside Cylinder 1 decreased, causing the water inside Cylinder 2 to move toward Cylinder 1 and, in turn, causing the piston in Cylinder 2 to move backward. By adjusting the position of the linear actuator, the piston inside Cylinder 2 could be controlled. A schematic diagram of experimental setup is shown in Figure 3.1.

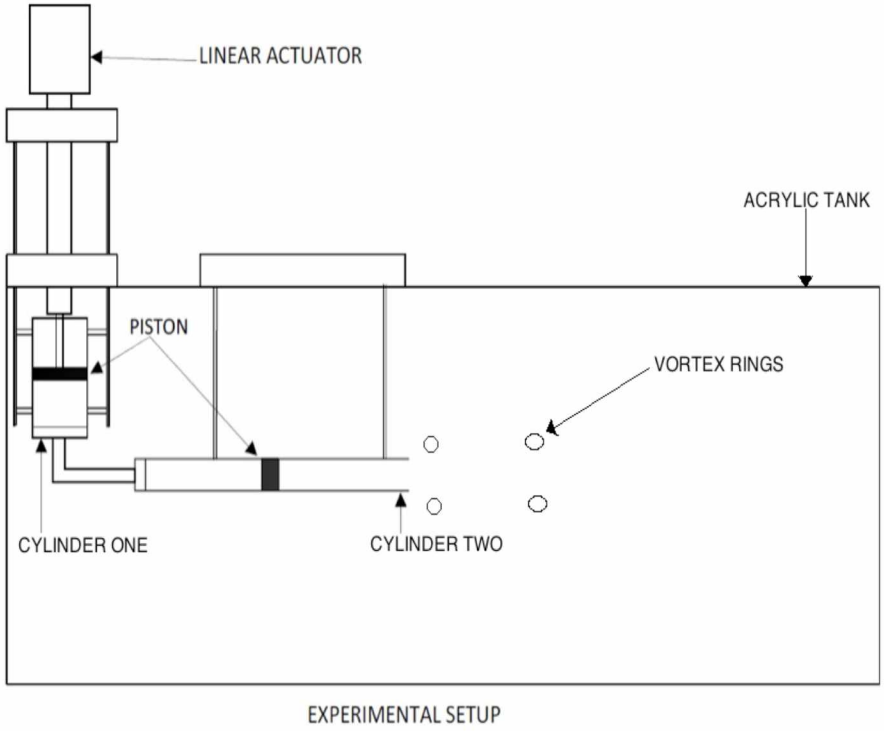

Figure 3.1 Schematic diagram of experimental setup

3.1.1 Modeling of experimental setup

The diameters of Cylinder 1 and Cylinder 2 were significant factors in the success of the experiment. The diameter of Cylinder 1 (0.05 m) was the diameter necessary to exert a force equivalent to 2 m of pressure on the piston head, the minimum force required to produce a single vortex ring, as described in the following formula:

Horizontal force = hydrostatic force acting on face of piston.

$P = \rho g h$

P = hydrostatic pressure

ρ = density of water = 1000kg/m^3

g = gravitational for= 9.81m/s^2

h = depth or height of liquid column = 2m

P = 1000*9.81*2

P = 19620 N/m^2

As we know

P = F/A

F = P*A

If the diameter of the piston is assumed to be 1 inch (1 inch = 0.0254 m),

$$A = \left(\frac{\pi}{4}\right) d^2$$

d = diameter of cylinder

$$A = \left(\frac{\pi}{4}\right) * (0.0508)^2$$

$$A = 0.00202 \text{ m}^2$$

$$F = 19620 * 0.00202$$

$$F = 39.766 \text{ N} \approx 40 \text{ N}$$

then the minimum amount of force of required to push the column of liquid inside the cylinder is 40 N.

In choosing the linear actuator, which was supplied by the Phidgets Company, the factors considered included the length of the stroke; the velocity; the maximum force; and the minimum force required, which, as calculated above, was 40 N. Even though the linear actuator could produce the minimum force required, the velocity that it could produce was relatively small for the experiments. To increase the velocity of the piston inside Cylinder 2, cylinders with different diameters (i.e., 0.05 m for Cylinder 1 and 0.025 m for Cylinder 2), one of which was two times larger than the other, were used. Due to this difference in diameter, the velocity of the piston in Cylinder 2 was four times that of the velocity of the piston in Cylinder 1.

The linear actuator was connected to a direct current (DC) motor controller, which controlled its DC gear motor, and to a personal computer (PC) using a control board.

Using a USB connecting port, the controller received pulses sent by a program written using Labview software, which operated the DC motor of the linear actuator accordingly. Accordingly, the board sent rated voltage to the DC motor in the linear actuator. To control the movement of the piston inside Cylinder 2, the velocity and acceleration of the piston in stroke had to be varied. By varying the input voltage to the linear actuator using a program written with Labview software, the velocity and acceleration of the linear actuator could be controlled. The Labview software

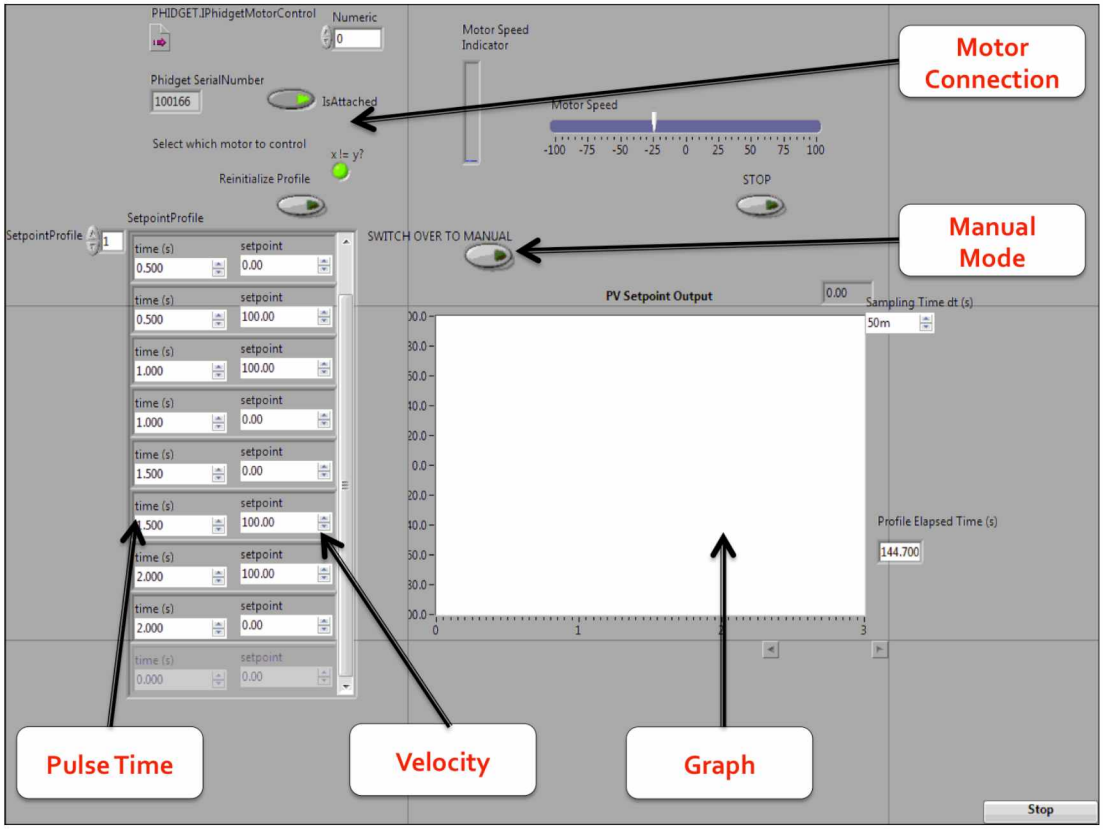

Figure 3.2 View of control panel of linear actuator

As can be observed, the control panel has four switch buttons. The button near the Phidget motor control displays whether the motor is connected, the button above the set

point profile is used to start the point profile, the button above the graph is used to switch between the manual mode and point profile modes, and the button near the speed indicator is used to stop the device. The motor speed knob is used to control the speed of motor in manual mode. The point profile generates a graph of the setpoint profile output. When the point profile switch is on, the program generates pulses according to points given in windows, which are then carried to the controller. The controller then varies the voltage according to the received input, with time point and velocity given as inputs into the program.

3.2 Velocity profile

Figure 3.3 shows the velocity profile of the piston in Cylinder 2, which was driven by the linear actuator. Two high constant peaks can be observed in the curve, which shows the velocity of piston over time. The timing of a constant peak determines the formation time of vortex rings such that as the peak time increases, the formation time of the ring increases. The extent of a decrease in the velocity between the peaks determines the non-dimensional frequency number of the rings, while the extent of the increase in the time gap between the rings determines the decrease in the non-dimensional frequency number. At the same time, the velocity of the piston determines the Reynolds Number of the vortex rings such that as the peak velocity increases, the Reynolds Number of the rings increases. The voltage, time gap, and time were varied in the control panel to change the profile of the piston until the values required to obtain vortex rings with the desired characteristics were obtained.

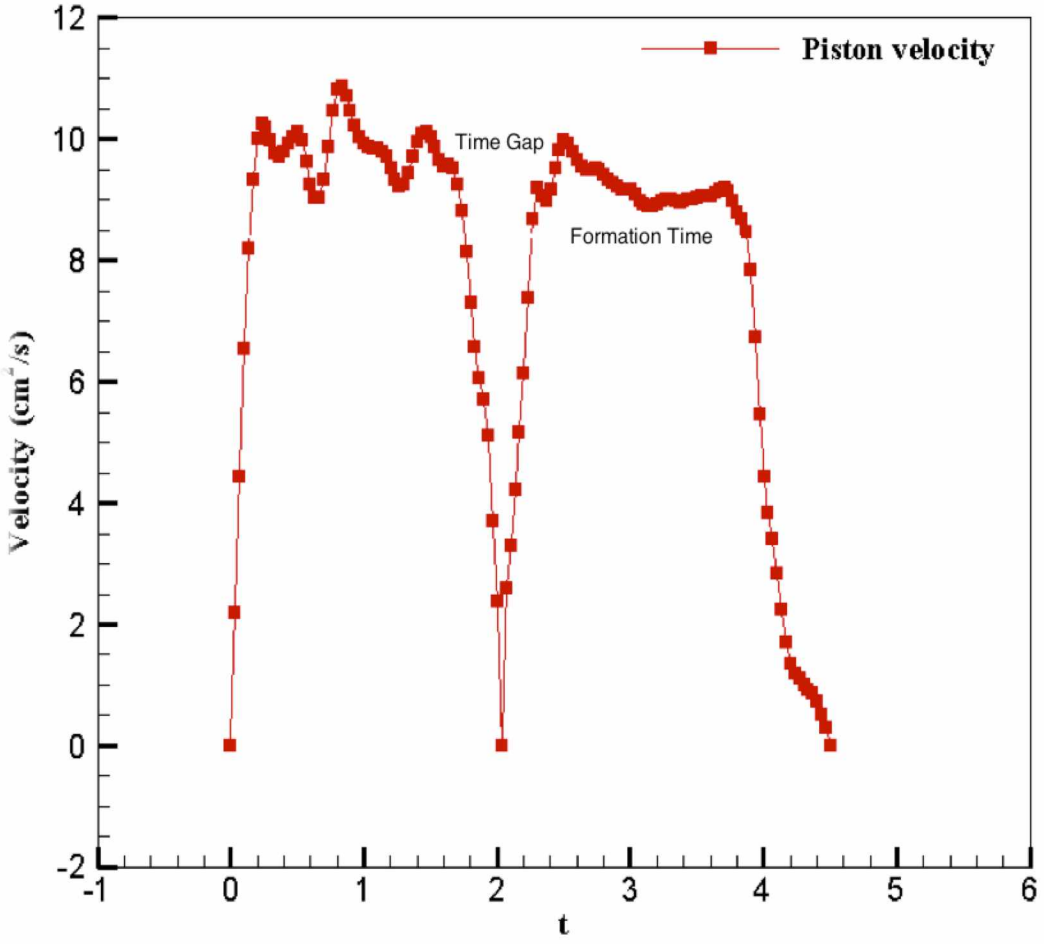

Figure 3.3 Velocity profile of the piston in Cylinder 2

3.3 Digital particle image velocimetry

Digital particle image velocimetry (DPIV) is a technique for measuring an entire instantaneous flow field. Using the DPIV, cross-correlation of a group of particles in the flow within a known interval is performed. These particles are then added to the flow in a process known as seeding. Although different types of particles are used, depending on the nature of the flow investigated, the particles selected should have a gravity very close to that of the fluid so that they move as if they were part of the fluid. To detect the seeding movement, an area of the flow field is illuminated by a light sheet, which is generated by a laser and a system of optical instruments, and the positions of the particles recorded on a digital CCD camera. Using a data processing method, such as the cross-correlation method, the average displacement of the particles within a small interrogation area between the pulses of the light sheet in the image is determined. Determination of the average displacement allows for determination of the interval between frames, and subsequently calculation of the 2-D velocity flow field. Finally, a post-data processing technique is applied to remove incorrect information and noise from the raw data to obtain a "refined" version of the velocity field. More detailed information regarding DPIV can be found in Raffel et al. (2007). In all experiments, in-house software was used to conduct the DPIV analysis necessary for performing cross correlation of the images and determining the velocity and direction of different points in a window.

3.3.1 Seeding

To obtain images of the flow field, the tank was seeded with silver-coated hollow glass beads that were sufficiently small to follow the flow but sufficiently large to be illuminated. In general, use of DPIV requires a high particle density; as a general rule, at least ten particles should be correlated for each measured velocity vector. The hollow silver-coated glass beads used in this study, which were manufactured by Potter Industries, had a mean diameter of 11 to 18 microns and a density of 1.1 g/cc.

3.3.2 Laser light sheet production

Figure 3.4 shows the neodymimum-Yttrium aluminum garnet laser setup that was used to generate a thin sheet of laser light plane. The laser had the following specifications:

- Output power: 250 mW–800 mW
- Pump diode: 2.5 Watt
- Diode make: nLight
- Wavelength: 532 nm (green)

The laser light was passed through a cylindrical lens to produce a thin sheet of laser that was used to illuminate the plane of measurement.

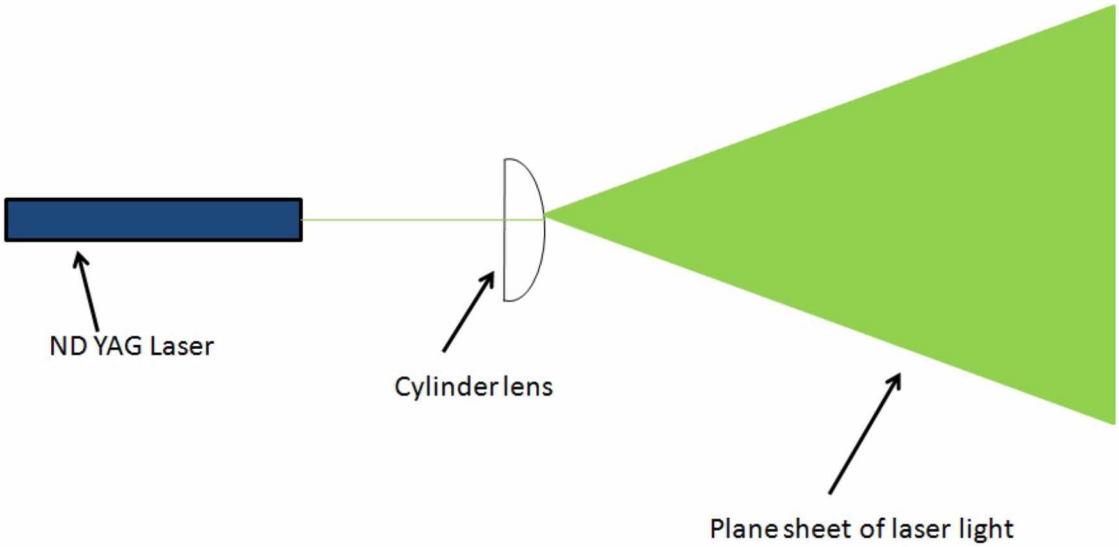

Figure 3.4 Schematic diagram of laser light sheet production

3.4 Experimental procedure

The experiments were conducted in a 1.5 × 0.6 × 0.6 m glass tank filled with clear water to a level at which both cylinders, and thus the system, were completely immersed. The thin laser sheet was manipulated to meet the exact center of the inner tube and the plane of the laser to align with the axis of inner cylinder. The camera was then positioned exactly perpendicular to the plane of the laser and the field of view set by the zoom function to cover the area in which the vortex rings interacted.

The linear actuator and movement of the pistons were controlled using a program written using Labview software, as previously described. If the correct values for time and speed were entered into the set point profile window, the linear actuator would push the piston accordingly. In order to reset the piston to the initial position, the mode was switched to manual so that the piston could be pulled back to the initial position and the

experiment could be repeated several times, which was necessary due to the highly instable nature of vortex rings.

The parameters of formation time, Reynolds Number, and non-dimensional frequency number were varied using the Labview program when repeating the experiment. By varying the timing of pulses in the Labview panel, different formation times could be obtained. By varying the voltage of pulses, the speed of the linear actuator could be varied to produce different Reynolds' numbers of rings. By varying the time gap in the pulses between rings, different non-dimensional frequency numbers could be produced between the rings. The CCD camera was set to begin recording the interaction between the rings after the profile had been set in the profile window and to stop recording when one or both of the rings passed out of view. The recording of the interaction between the rings stored in the camera's memory was later copied to a laboratory computer and converted into series of images for DPIV analysis. As the camera recorded at 30 frames per second, 30 images were obtained for each second of recording.

3.4.1 DPIV processing

In-house software was used to perform DPIV processing. As this software accepts only raw images as inputs, a Matlab code was used to convert the images into a raw format. Using this software, a .par file was created that contained all the data regarding the window size, cross-correlation distance, pixel ratio, and image dimensions. Using this file as an input, a Perl script was used to analyze the images and produce .vel and .vor files of the images, which could be plotted and measured using Matlab software.

DPIV processing was performed using the cross-correlation technique. The sub regions were 32 × 32 pixels and had a 50% overlap, and the pixel resolution was calculated for each experiment manually (Raffel et al. 2007). As required for processing, a .par file with a preset interrogation region size, image size (1920 × 1080 pixels), and pixel resolution was created. Figure 3.5 shows the schematic diagram of DPIV processing used in the following experiments.

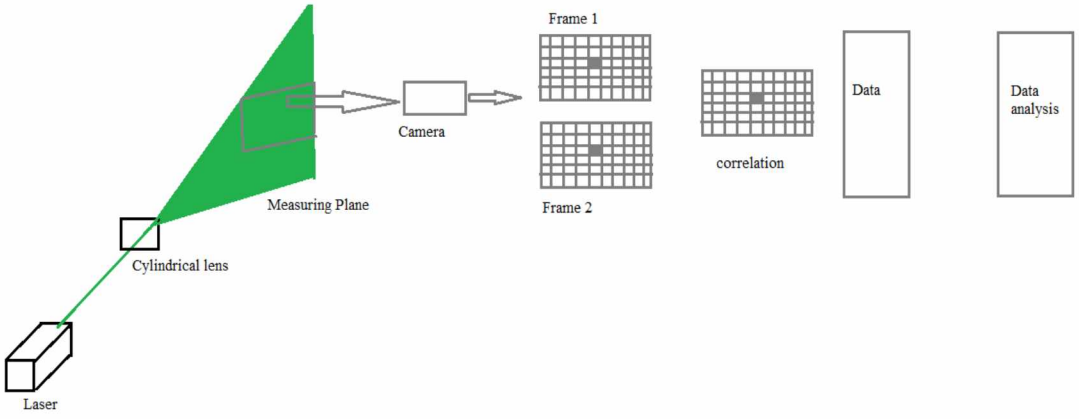

Figure 3.5 Schematic diagram of DPIV processing

3.5 Data collection

To measure the circulation for each frame, Matlab software was used to measure the area integration of vorticity on the vorticity plot of the vortex rings. After the .vel and .vor files had been converted to Matlab-compatible files, they were plotted using Matlab. To identify the trajectory of the vortex rings, which was considered the center of the vortex rings and the point of highest vorticity, the point at which the vortex level was high was determined.

When measuring the circulation of vortex rings, different states appear as the rings move. During some states, the software may consider both rings to be one ring, especially when they come close to each other. At an elongated ring in the plot, the measurement contour is defined at an area where clear necking is observed. If necking cannot be observed, then the contour is defined at mid-distance between the vortex rings. The two cases and the respective measurement contours are shown in Figures 3.6 and 3.7.

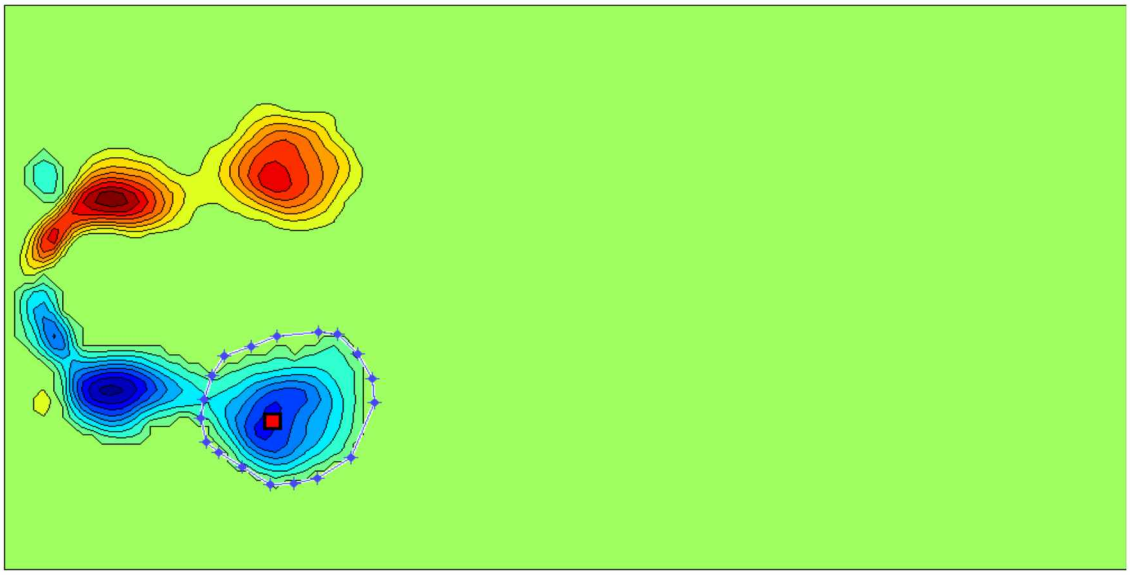

Figure 3.6 Circulation contour definition where necking is observed in an elongated ring

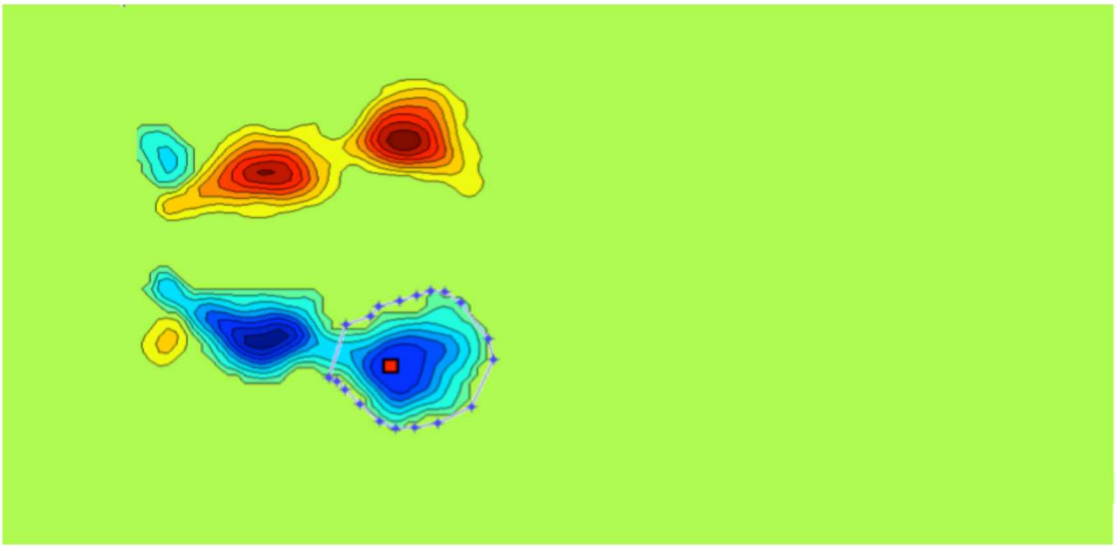

Figure 3.7 Circulation contour definition where necking is not observed in an elongated ring

Chapter 4 Results

4.1 Present work

As discussed in the literature review, a wide range of fascinating questions regarding vortex dynamics in general and the dynamics of the interaction between vortex rings in particular have either not been addressed or have been only partially addressed. To assist in addressing these questions, this study observed the interaction between a coaxial and a co-rotating vortex ring under various conditions to investigate the following issues:

- The behavior of the vortex rings pre- and post-interaction
- The trajectory of the vortex rings during interaction
- The effect of the leading ring on the trailing ring
- The changes in the circulation of the leading and the trailing ring with variations in the parameters of non-dimensional frequency, Reynolds Number, and formation time
- The nature of the leapfrogging process that results from the interaction between the coaxial and the co-rotating vortex ring

4.2 Experiments

The objective of the experiments was to investigate the changes in the dynamics of the interaction between a coaxial and a co-rotating vortex ring with changes in the parameters of non-dimensional frequency, Reynolds Number, and formation time. To do so, the experiments conducted at each formation time examined were repeated at different Reynolds Numbers, and the experiments conducted at each Reynolds Number were then repeated at different non-dimensional frequency numbers. As the formation time is defined as ratio of the stroke length of a piston to the diameter of a tube, it can be varied by varying the stroke, and was done so to yield the Formation Times 1.5, 2, and 3, the values examined in this study. These values were chosen because the total formation times for two interacting rings have been found to be 3, 4, and 6, which are below, equal to, and above, respectively, the optimum formation time for vortex rings in a piston–cylinder system (Gharib et al. 1998). As the stoke length is directly proportional to the time period of a given pulse, the length could be increased by increasing the time pulse in the Labview control panel until the correct value had been obtained.

The Reynolds Number is determined by the magnitude of voltage provided to the linear actuator such that the higher the magnitude, the higher the Reynolds Number. At each formation number, the experiments were repeated at different Reynolds Numbers, which had been created by varying the magnitude of the voltage provided to the linear actuator. The time gap between the pulses, each of which related to a ring, determined the non-dimensional frequency number of the interaction between the rings. Different non-

dimensional frequency numbers were examined at the same formation time and Reynolds Number. A diagram of the experimental process is shown in Figure 4.1.

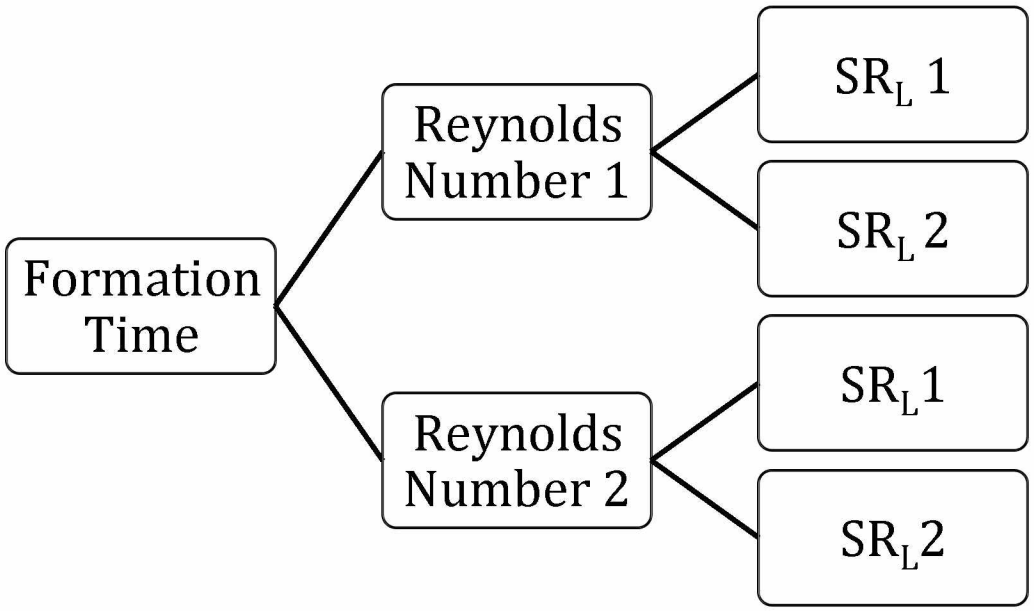

Figure 4.1 Schematic diagram of the experimental process

In studying the dynamics of the interaction between coaxial and co-rotating vortex rings, the vortex rings follow each other in the interaction time. It is thus important that the vortex rings not lose vorticity before interacting. Gharib et al. (1998) found that the optimum vortex ring is formed at Formation Time 4, which implies that no vorticity shedding should be observed at a formation time less than 4. As no loss of vorticity in individual rings was observed using Formation Times 1.5, 2, and 3 in this study, the results confirm Gharib et al. (1998)'s findings.

4.3 Formation Time 1.5

4.3.1 Vortex plot

Figure 4.2 and 4.3 shows a vortex plot of the interaction between the coaxial and co-rotating vortex rings at Formation Time 1.5. The different time steps are noted with the numbers 1 and 2. At the Time Step 1.1678 seconds, the fully developed Vortex Ring 1 can be observed. At Time Step 2.1678 seconds, the developing trailing Vortex Ring 2 can be observed. At Time Step 3.1698 seconds, the two fully developed Vortex Rings 1 and 2 can be observed, with Vortex Ring 2 moving toward the center of Vortex Ring 1. At Time Step 4.170 seconds, Vortex Ring 2 can be observed moving toward the center of Vortex Ring 2.

At Time Step 5.171 seconds, Vortex Ring 2 passed through Vortex Ring 1 as the rings underwent leapfrogging. At Time Step 6.171 seconds, Vortex Rings 1 and 2, partially merged but retaining distinct cores, underwent leapfrogging for a second time. At Time Step 7.178 seconds, the two rings continued leapfrogging. At Time Step 8.174 seconds, two separate vortex rings can be observed, as had been observed at Time Step 3.169 s. At Time Step 9.174 seconds, Vortex Ring 1 tries to move toward the center of Vortex Ring 2. At Time Step 10.174 seconds, Vortex Ring 1 comes between Vortex Ring 2. At Time Step 11.178 seconds, the vortex rings completely merge into one ring.

As can be observed from the plot, the level of vorticity decreased as the rings passed each other, with a particularly sharp decrease in the vorticity of the trailing ring occurring at 7.137 seconds. This result indicates that the trailing ring was losing

circulation by vortex shedding, the explanation for which is explored in the following section. It can also be observed that the rings underwent leapfrogging twice with no strong shedding of vorticity from the trailing ring as the rings passed each other. Whereas leapfrogging occurred at lower Reynolds Numbers and higher non-dimensional frequency numbers, no leapfrogging occurred at higher Reynolds Numbers and lower non-dimensional frequency numbers.

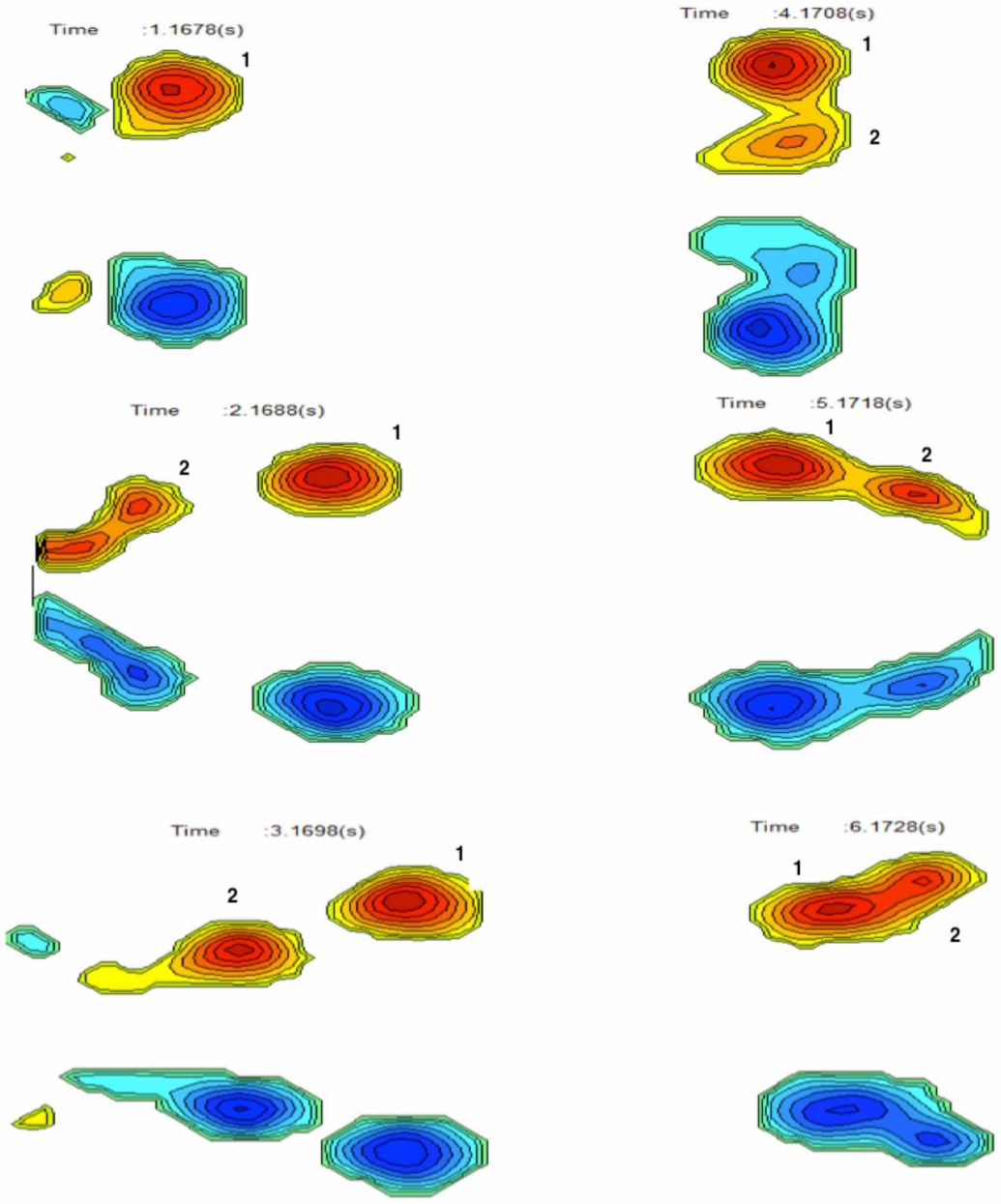

Figure 4.2 Vortex plot of coaxial–co-rotating vortex ring interaction at Formation Time 1.5, Reynolds Number 2836, and SR_L 0.8

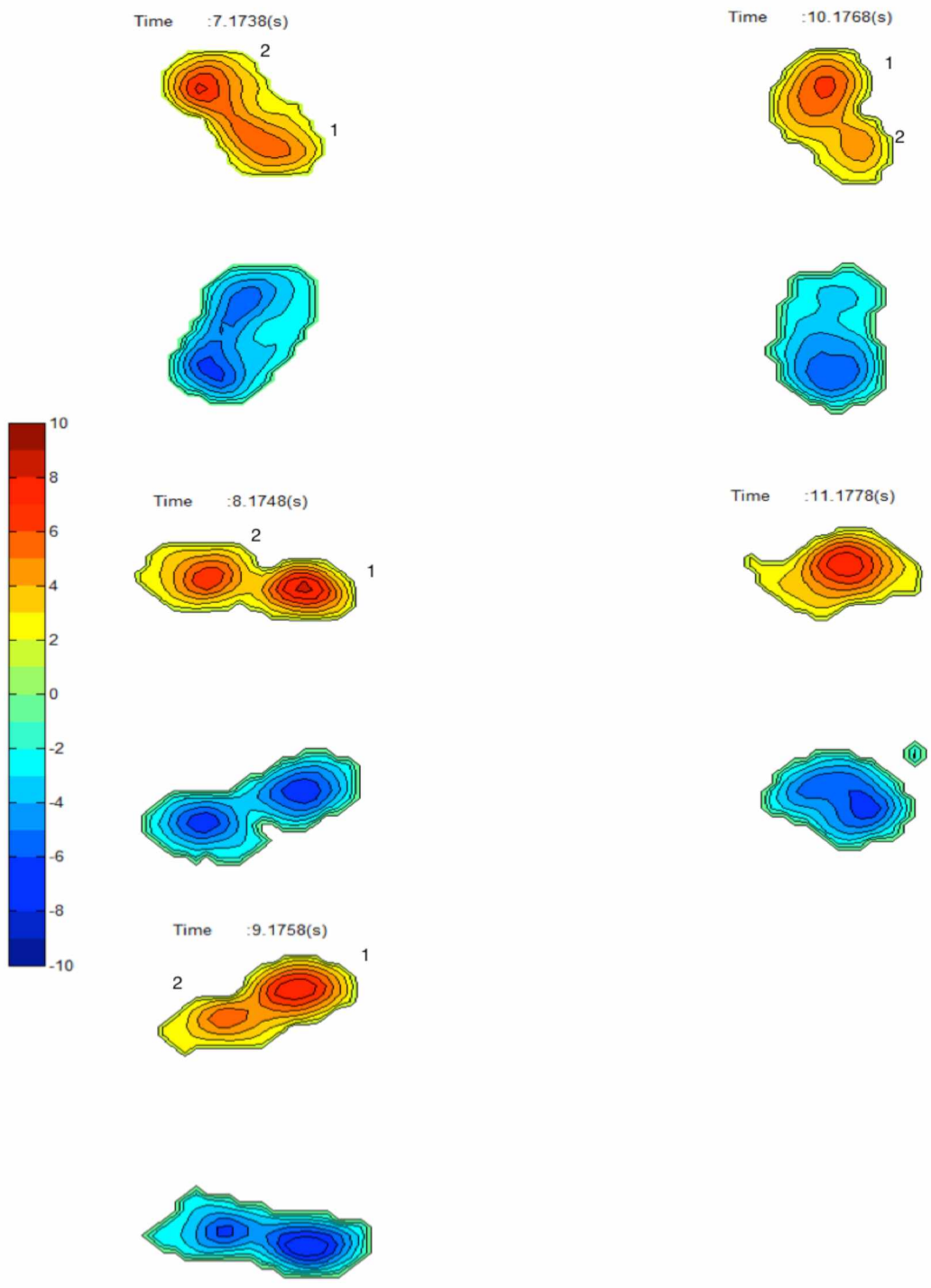

Figure 4.3 Vortex plot of coaxial–co-rotating vortex ring interaction at Formation Time 1.5, Reynolds Number 2836, and SR_L 0.8

4.3.2 Trajectory of vortex rings

Figure 4.4 shows the trajectory of the vortex rings. The Vortex Ring 1 curve shows the path of the center of the leading ring and the Vortex Ring 2 curve shows the path of the center of the trailing ring center in the interaction between the coaxial and co-rotating vortex rings. Once the leading ring had fully developed, it began moving horizontally. Although the trailing ring had begun to develop, the rings did not move in the same vertical direction, indicating that the trailing ring had not fully developed. While the center of the leading ring center began moving upward, indicating that it was expanding, the center of the trailing ring began moving downward, indicating that it was compressing while trying to come closer to the first ring. The center of the leading ring then began to move downward while the center of the trailing ring began to move upward, indicating that the leading ring was compressing while the trailing ring was expanding, until the two rings eventually changed positions by undergoing leapfrogging. After they had completed leapfrogging, the leading ring became the trailing ring while the trailing ring became the leading ring. The rings then began to repeat the process of expanding and compressing until they eventually changed positions again by undergoing leapfrogging for a second time. After they had completed leapfrogging for the second time, the trailing ring began losing circulation to a significant extent.

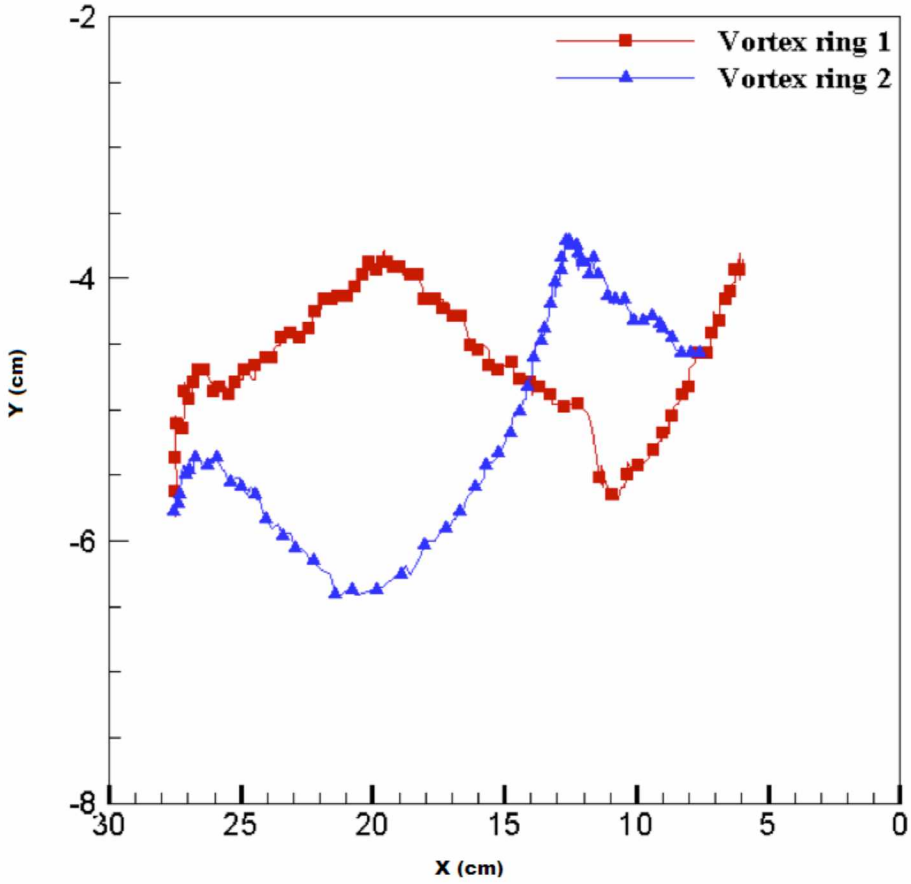

Figure 4.4 Vortex ring trajectory at Formation Time 1.5

4.3.3 Circulation at Formation Time 1.5

Figure 4.5 shows the circulation plot of the vortex rings at Reynolds Number 2836 and SR_L 0.8. For both the leading and the trailing ring, an increase in circulation was initially observed, indicating the development of both rings. After the circulation of the rings had reached maximum, the circulation of the leading ring remained constant, while the circulation of the trailing ring began to decrease. After undergoing leapfrogging, the circulation of the trailing ring began to increase, indicating that it was trying to regain circulation, while the circulation of the leading ring decreased after undergoing leapfrogging. This circulation trend was not observed for all the vortex rings examined at Formation Time 1.5. At higher Reynolds Numbers and lower non-dimensional frequency numbers, the rings attempted to undergo leapfrogging, but were unable to complete a leapfrogging cycle. Whereas the circulation of the leading ring remained constant, irrespective of the Reynolds Number and the non-dimensional frequency number, the circulation of the trailing ring decreased with an increase in the Reynolds Number.

The dx curve in the plot shows the stream-wise separation of the vortex rings, illustrating how the rings moved horizontally over time, while the dy curve shows how the rings moved vertically over time. Analysis of the dx curve trend allowed for identification of curve behavior. At Formation Time 1.5, the dx curve clearly shows that the rings had undergone leapfrogging. The dx curve initially decreased, indicating that the trailing ring was trying to move toward the center of the leading ring, after which the dy curve increased, indicating that the rings were returning to their normal positions. The curve

remained constant for some time before beginning to decrease again, indicating that the trailing ring was trying to pass through the leading ring again. The dx curve reveals that as the rings moved horizontally over time, the distance between the rings initially decreased, indicating that the rings were coming closer to each other. After undergoing leapfrogging, the distance between them increased, indicating that the rings were moving apart. After reaching a peak at 5 seconds, the distance between the rings began to decrease again, indicating that they were trying to undergo leapfrogging yet again. These results indicate that the number times that vortex rings undergo leapfrogging is equal to the number of times that the dx and dy curves cross the axis.

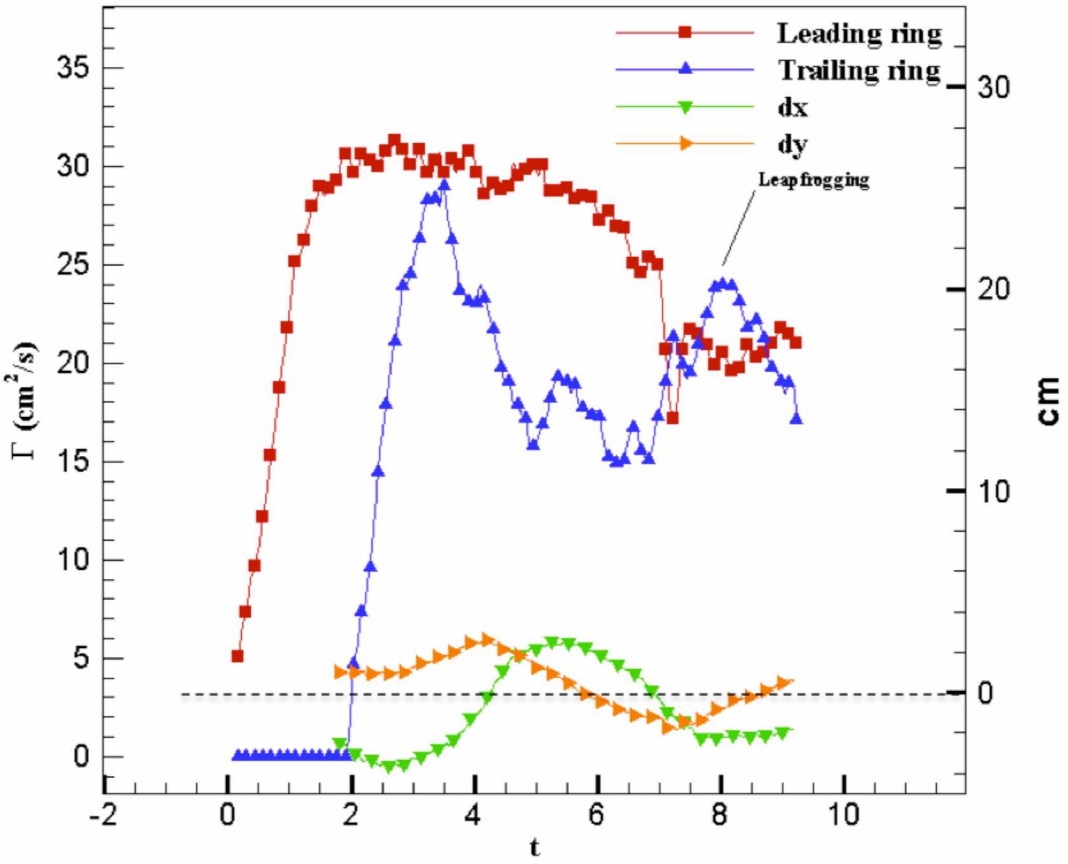

…

Figure 4.5 Vortex ring circulation at Formation Time 1.5, Reynolds Number 2836, and SR_L 0.8

4.3.4 Reynolds Number

The experiments at Formation Time 1.5 were repeated at different Reynolds Number of 2801, 4763, 6414, and 8243, and the experiments at each Reynolds Number were repeated at different non-dimensional frequency numbers. The results of all the experiments are discussed in the following sections.

4.3.4.1 Reynolds Number 2801

Leading rings

Figure 4.6 shows the circulation curves of the leading rings at Formation Time 1.5, Reynolds Number 2801, and SR_L 0.8, 0.705, 0.631, and 0.545. As can be observed, the circulation of the leading ring throughout the interaction between the coaxial and co-rotating vortex rings remained constant at all non-dimensional frequency numbers except at SR_L 0.8. The reason for this difference at SR_L 0.8 is that the rings underwent leapfrogging at this non-dimensional frequency number, in accordance with the detailed explanation of leapfrogging and ring trajectory provided in the previous section.

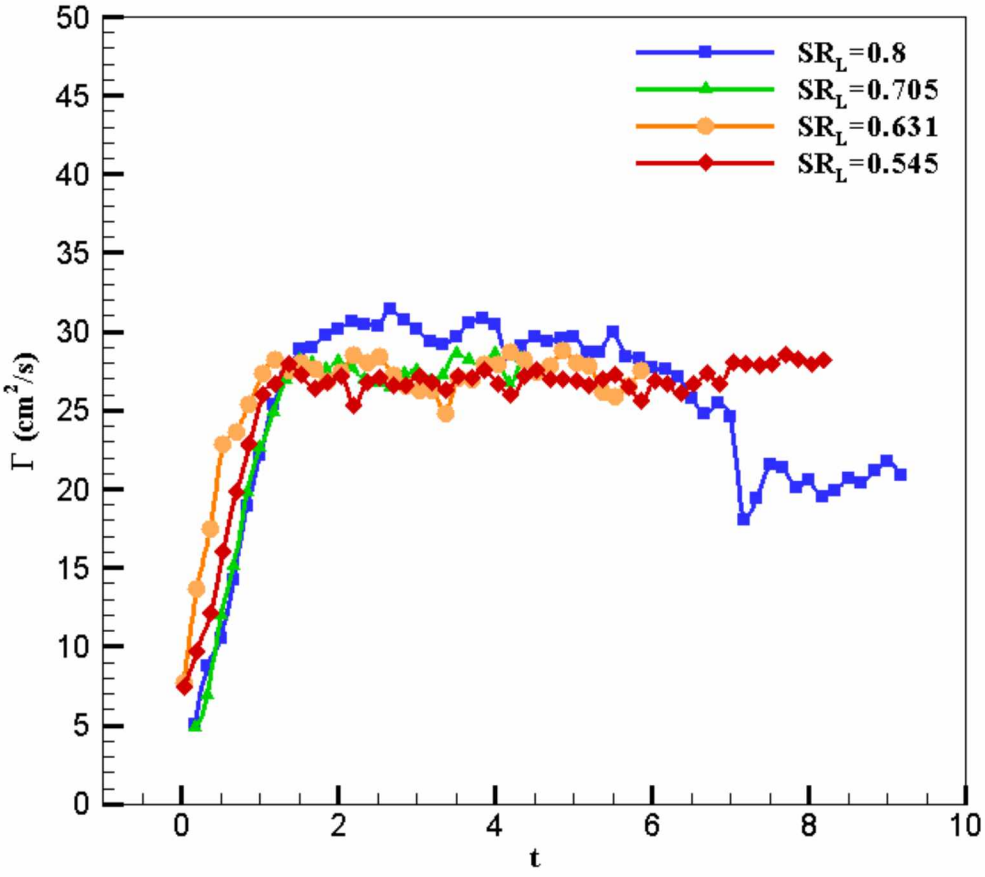

Figure 4.6 Leading ring circulation at Formation Time 1.5 and Reynolds Number 2801

Trailing rings

Figure 4.7 shows the circulation of the trailing rings at Formation Time 1.5, Reynolds Number 2801, and SRL 0.8, 0.706, 0.631, and 0.545. As can be observed, the rate of increase in circulation was similar for all the rings except for the rings at SR_L 0.8 because the rings underwent leapfrogging at this non-dimensional frequency number. There was no constant phase in circulation of rings as in leading rings. After reaching a maximum, the circulation of the rings began to decrease at a rate that depended on the non-dimensional frequency number. Except for those at SR_L 0.8, the trailing rings at high non-dimensional frequency numbers experienced a higher rate of circulation loss. The curves show that as the non-dimensional frequency number decreased, the total circulation of the trailing ring increased except at SR_L 0.8, due to leapfrogging. The reason for this behavior is that as the non-dimensional frequency number increases, the amount of time that each ring has available for developing decreases, decreasing the time gap between the development of each successive ring, and thus decreasing the capacity of the trailing ring to gain circulation.

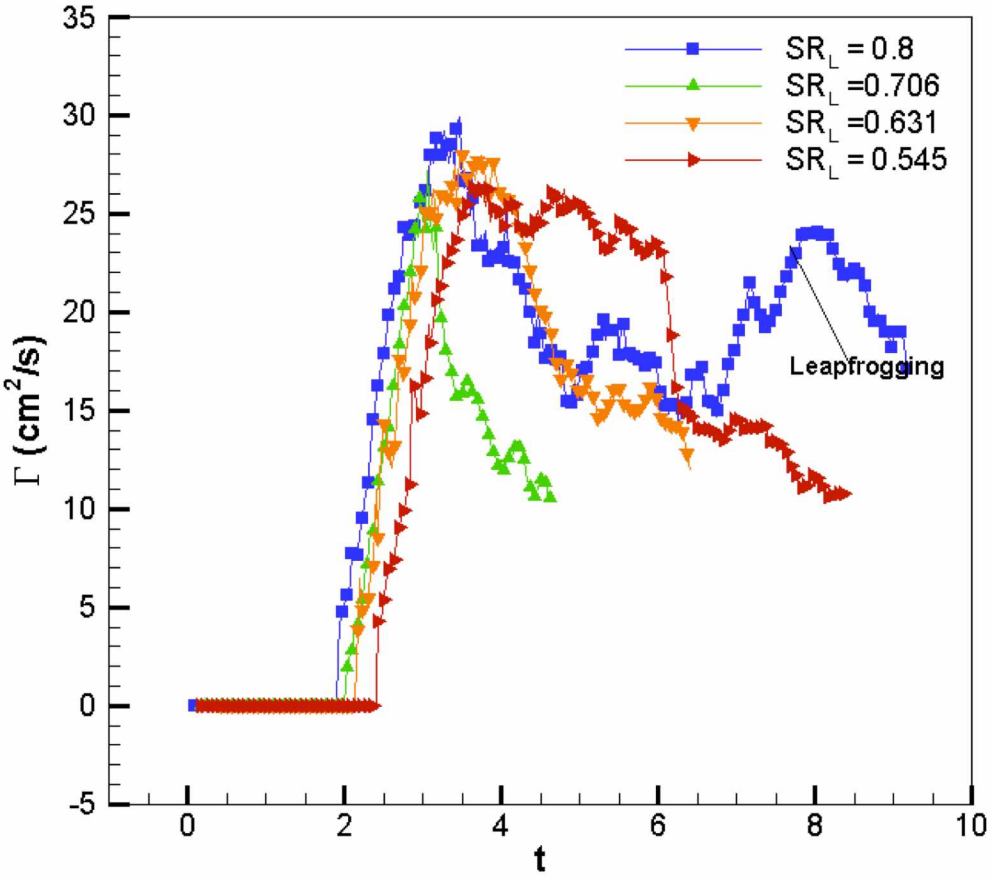

Figure 4.7 Leading ring circulation at Formation Time 1.5 and Reynolds Number 2801

4.3.4.2 Reynolds Number 4747

Leading rings

Figure 4.8 shows the circulation of the leading rings at Formation Time 1.5, Reynolds Number 4747, and SR_L 0.7, 0.583, and 0.5. As can be observed, the circulation

of the leading rings remained constant at all three non-dimensional frequency numbers. The rings at SR_L 0.583 and 0.5 showed the same pattern in development and attainment of maximum circulation, whereas the rings at SR_L 0.7 merged relatively early due to small time gap between the rings.

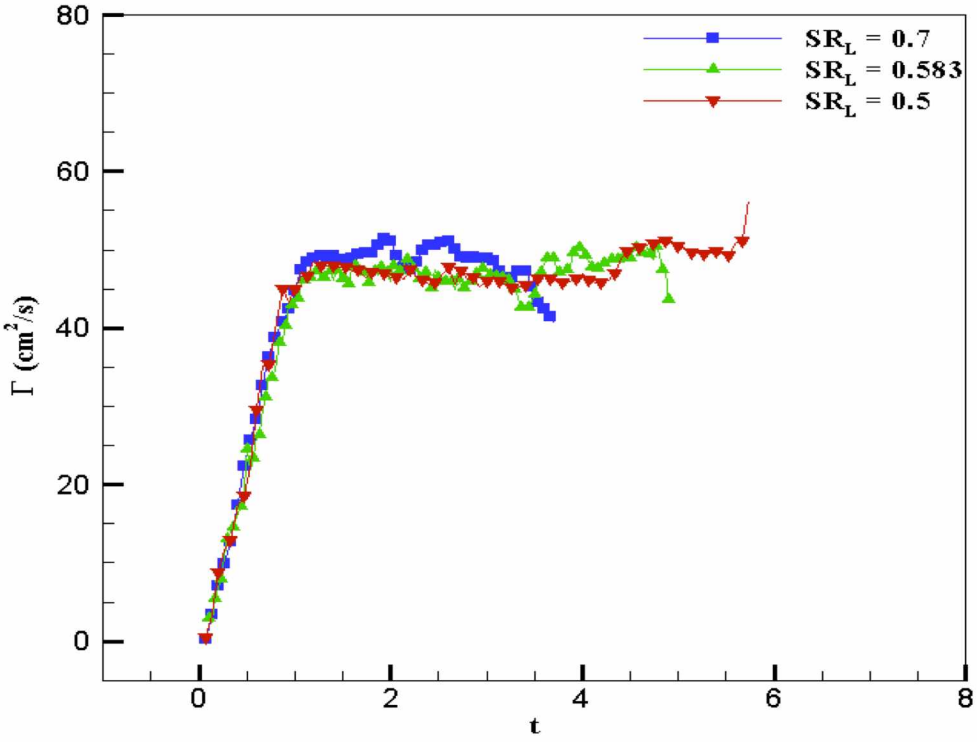

Figure 4.8 Leading ring circulation at Formation Time 1.5 and Reynolds Number 4747

Trailing rings

Figure 4.9 shows the circulation of the trailing rings at Formation Time 1.5, Reynolds Number 4763, and SR_L 0.7, 0.583, and 0.5. As can be observed, the trailing rings showed a similar circulation pattern at SR_L 0.583 and 0.5, whereas the trailing ring

at Reynolds Number 4763 and SR_L 0.7 began losing circulation relatively early. The increase in maximum circulation observed for rings at lower non-dimensional frequency number can be attributed to the increase in the time gap between the rings, which provided more time for the trailing ring to develop. These results indicate that as the non-dimensional frequency number decreases, the maximum circulation of the trailing ring increases.

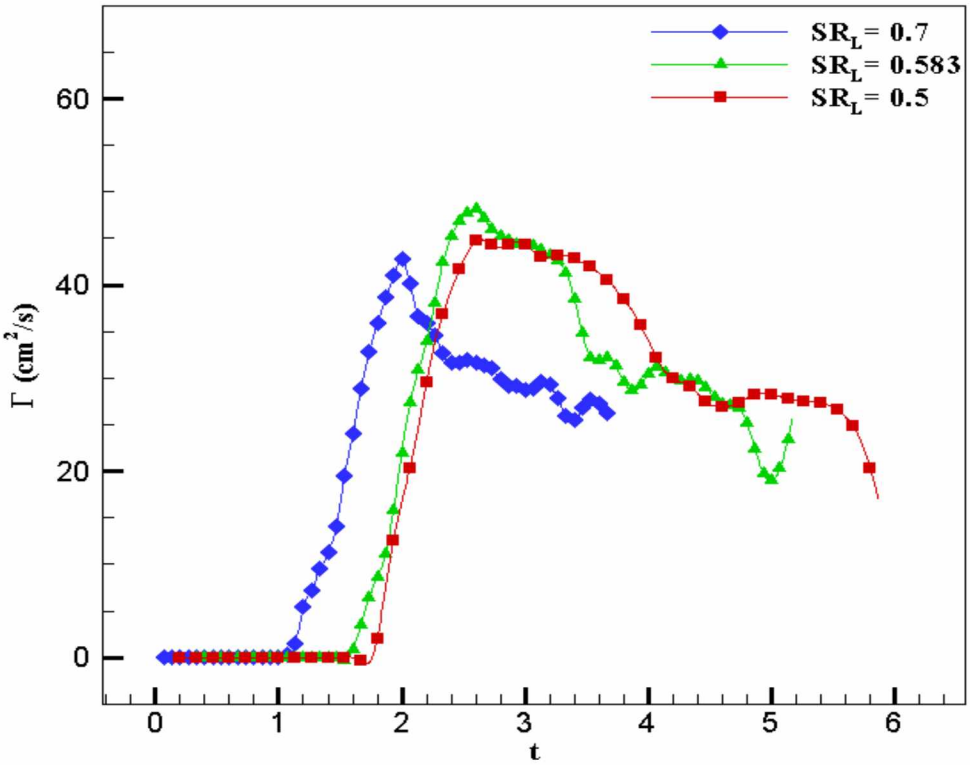

Figure 4.9 Trailing ring circulation at Formation Time 1.5 and Reynolds Number 4763

4.3.4.3 Reynolds Number 6414

Leading rings

Figure 4.10 shows the circulation of the leading rings at Formation Time 1.5, Reynolds Number 6414, and SR_L 0.571, 0.444, and 0.363. As can be observed, the circulation of the leading rings for Reynolds Number 6414 remained generally constant despite some fluctuations in circulation at SR_L 0.571, as the rings were trying to undergo leapfrogging at this higher dimensional frequency number.

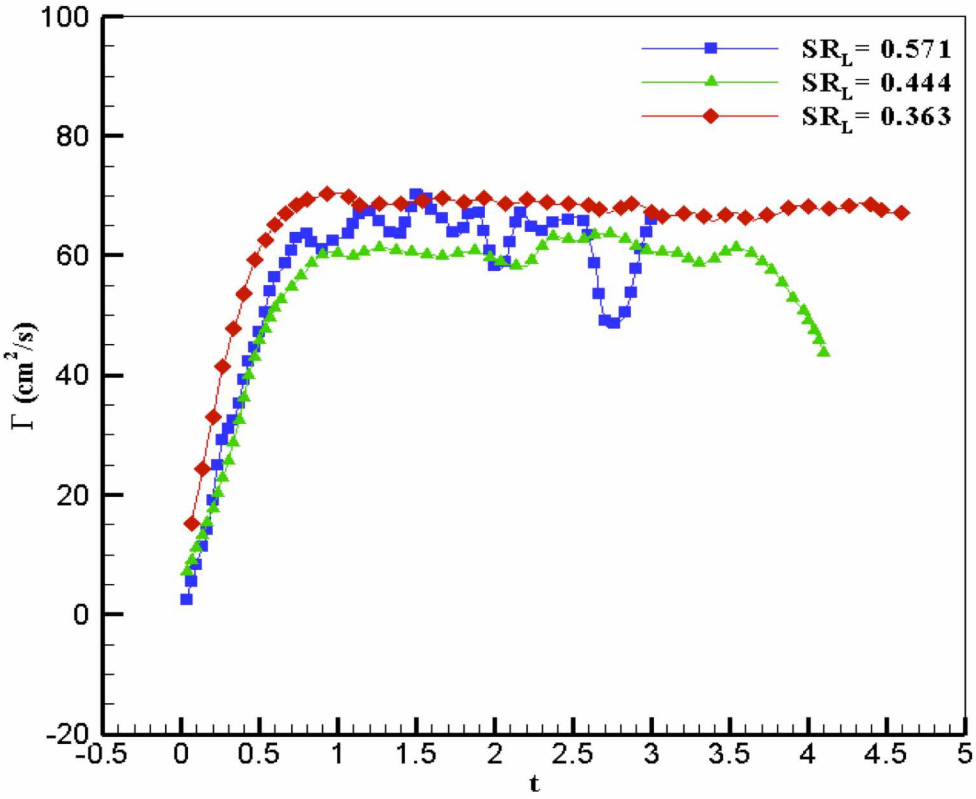

Figure 4.10 Leading ring circulation at Formation Time 1.5 and Reynolds Number 6414

Trailing rings

Figure 4.11 shows the circulation of the trailing rings at of Formation Time 1.5, Reynolds Number 6414, and SR_L 0.571, 0.444, and 0.363. A tendency for rings at lower non-dimensional frequency numbers to undergo leapfrogging, as well as a pattern of decrease and increase in the circulation of the trailing rings, can be observed. These results indicate that as the Reynolds Number increases, the probability that the rings will attempt to undergo leapfrogging increases. However, as the Reynolds Number increases, the rate at which the rings lose circulation increases, decreasing the ability of the rings to undergo leapfrogging. Thus, rings at a higher Reynolds Number are more likely to attempt to undergo leapfrogging, but are unlikely to be able to complete the leapfrogging process due to a loss in circulation.

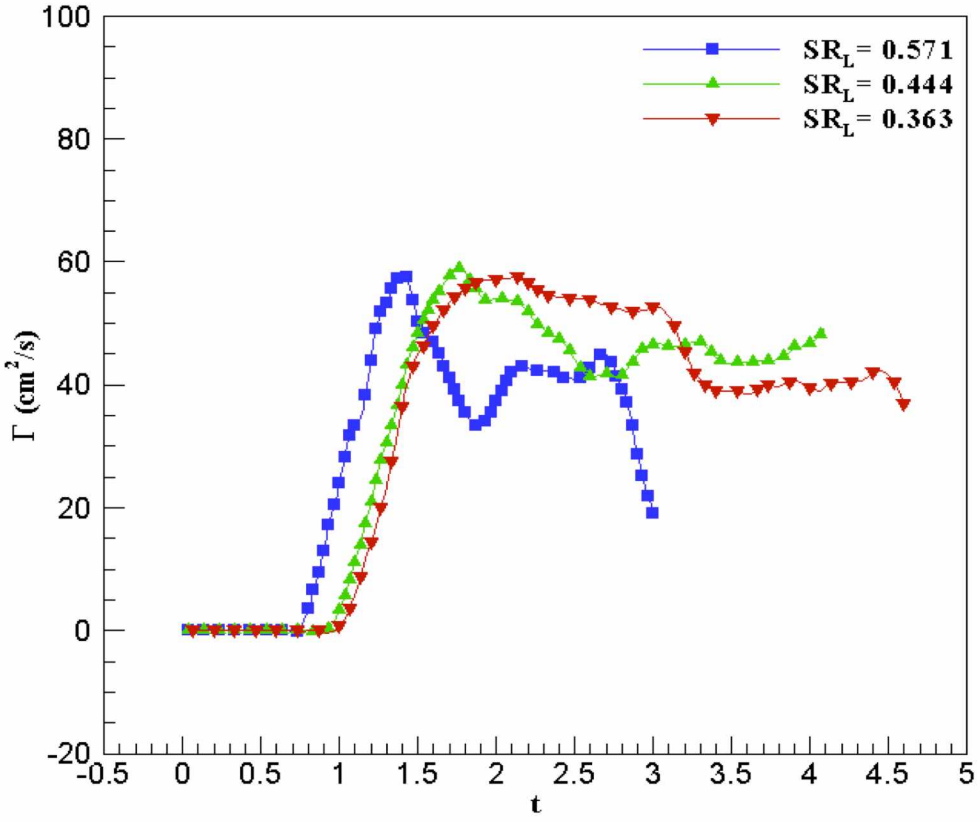

Figure 4.11 Trailing ring circulation at Formation Time 1.5 and Reynolds Number 6414

4.3.4.4 Reynolds Number 8243

Leading rings

Figure 4.12 shows the circulation of leading rings at Formation Time 1.5, Reynolds Number 8243, and SR_L 0.5, 0.428, 0.375, and 0.3. As can be observed, although the leading rings at Reynolds Number 8243 show a constant circulation, the rings at higher non-dimensional frequency numbers lose circulation relatively more rapidly. This difference is due to the fact that rings at higher non-dimensional frequency numbers are very close to each other, leading the interaction between them to be stronger, and causing some fluctuation in the circulation of the leading ring. In contrast, as the non-dimensional frequency number decreases, the gap between the rings increases, increasing the constancy of the circulation of the leading ring.

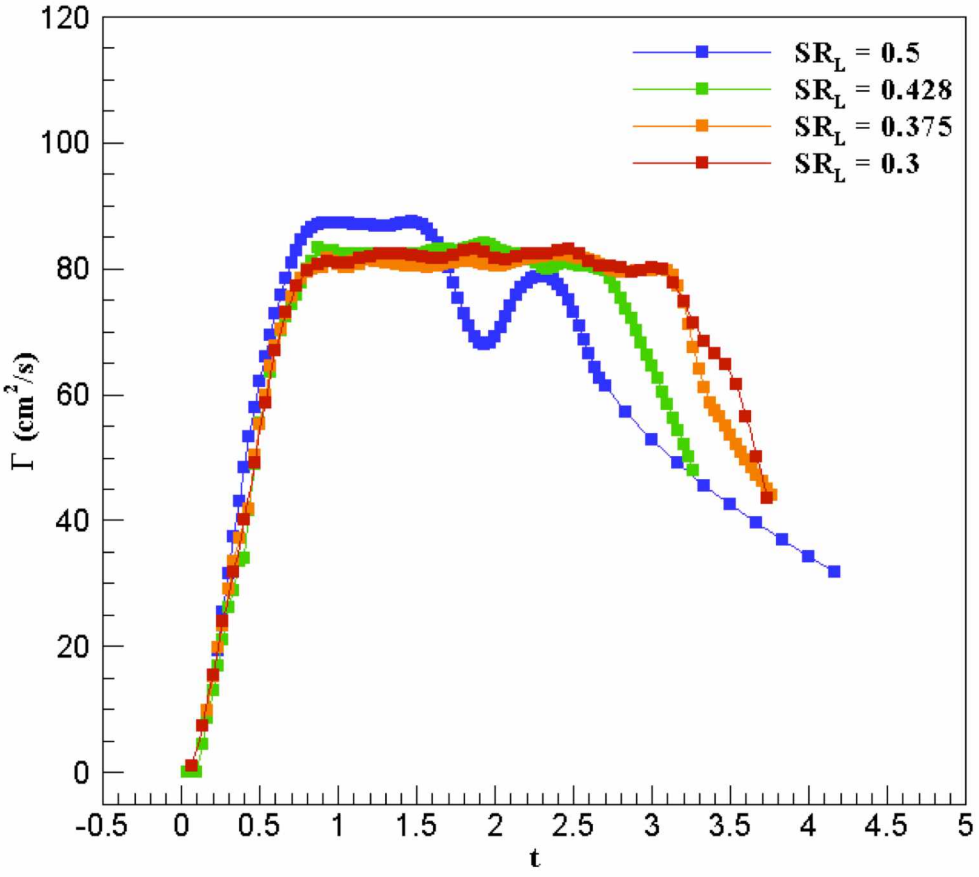

Figure 4.12 Leading ring circulation at Formation Time 1.5 and Reynolds Number 8243

Trailing rings

Figure 4.13 shows the circulation of trailing rings at Formation Time 1.5, Reynolds Number 8243, and SR_L 0.5, 0.428, 0.375, and 0.3. As can be observed, the pattern of the trailing rings is similar to that at Reynolds Number 6414, with the rings at higher non-dimensional frequency numbers showing a tendency to undergo leapfrogging.

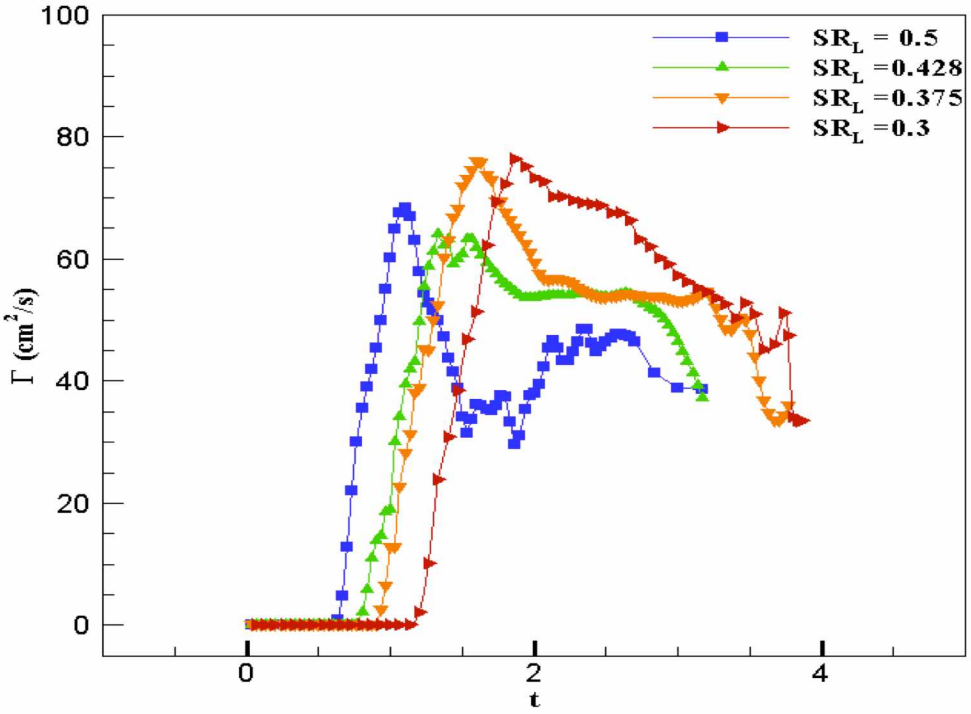

Figure 4.13 Trailing ring circulation at Formation Time 1.5 and Reynolds Number 8243

4.4 Formation Time 2

4.4.1 Vortex plot

Figures 4.14, 4.15 and 4.16 shows the interaction between the coaxial and co-rotating vortex rings at Formation Time 2 at different time steps in the experiments. As can be observed, development of the leading ring occurred from Time Steps 0.5 to 1.5 seconds, development of the trailing ring from Time Steps 2.5 to 3 seconds, and a decrease in the circulation of the trailing ring from Time Steps 3.5 to 4 seconds.

As shown in the vortex plot, elongation of the leading ring was observed over time. As shown in the circulation plot, a decrease in the circulation of the trailing ring and an increase in the circulation in the leading ring was observed over time, indicating that the leading ring absorbed some of the circulation of the trailing ring. From Time Steps 5 to 6.5 seconds, the trailing ring completely disappeared while the leading ring remained elongated, indicating that although part of the trailing ring was close to the leading ring, the rings had not completely merged. As the software could not distinguish between the rings because they were so close to each other, it displayed the two rings as a single elongated ring. As shown in the vortex plot, the trailing ring slowly merged with the leading ring at Time Steps 6 to 7.5 seconds to form a single ring, with no strong shedding of vorticity from the trailing ring observed. The vortex plots of the other experiments at Formation Time 2 reveal that no significant shedding of vorticity was observed in any of the experiments at this formation time.

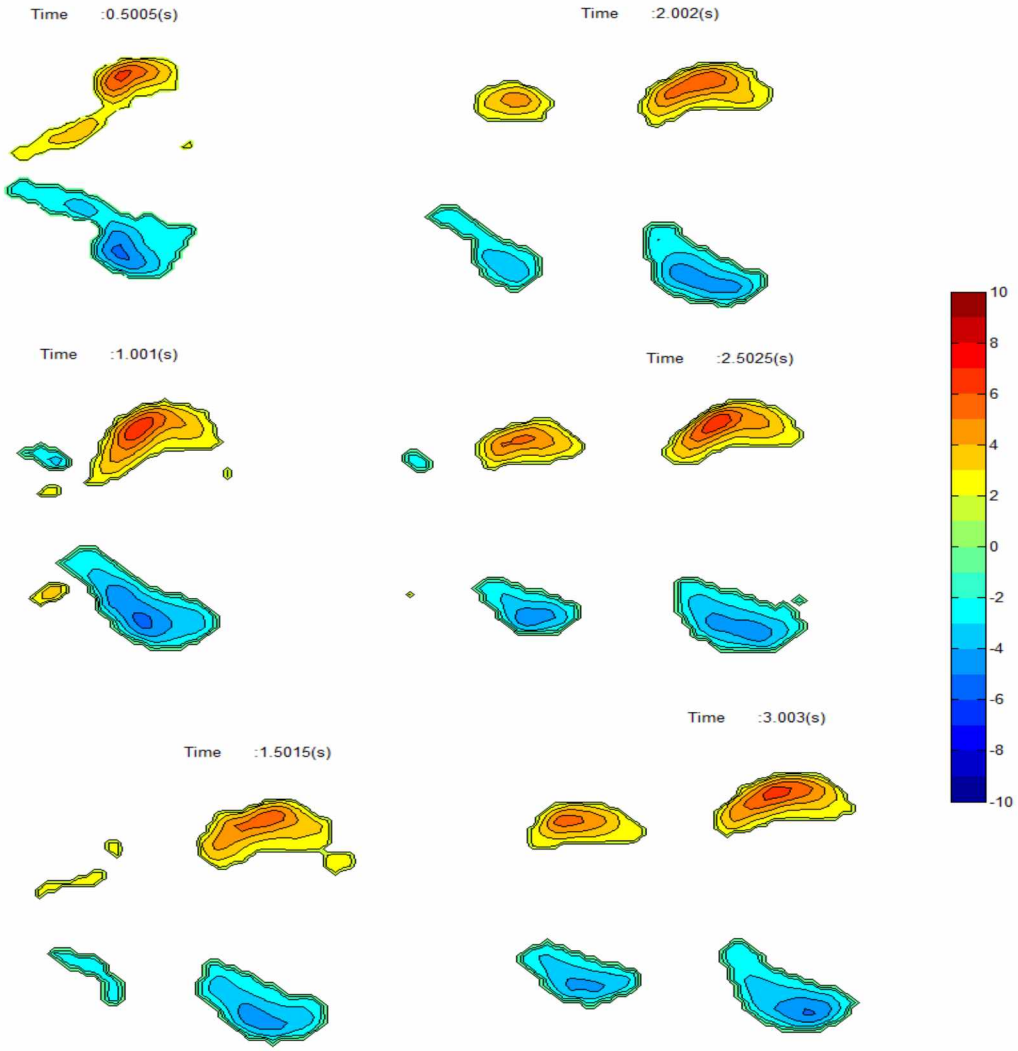

Figure 4.14 Vortex plot at Formation Time 2, Reynolds Number 5164, and SR_L 0.667

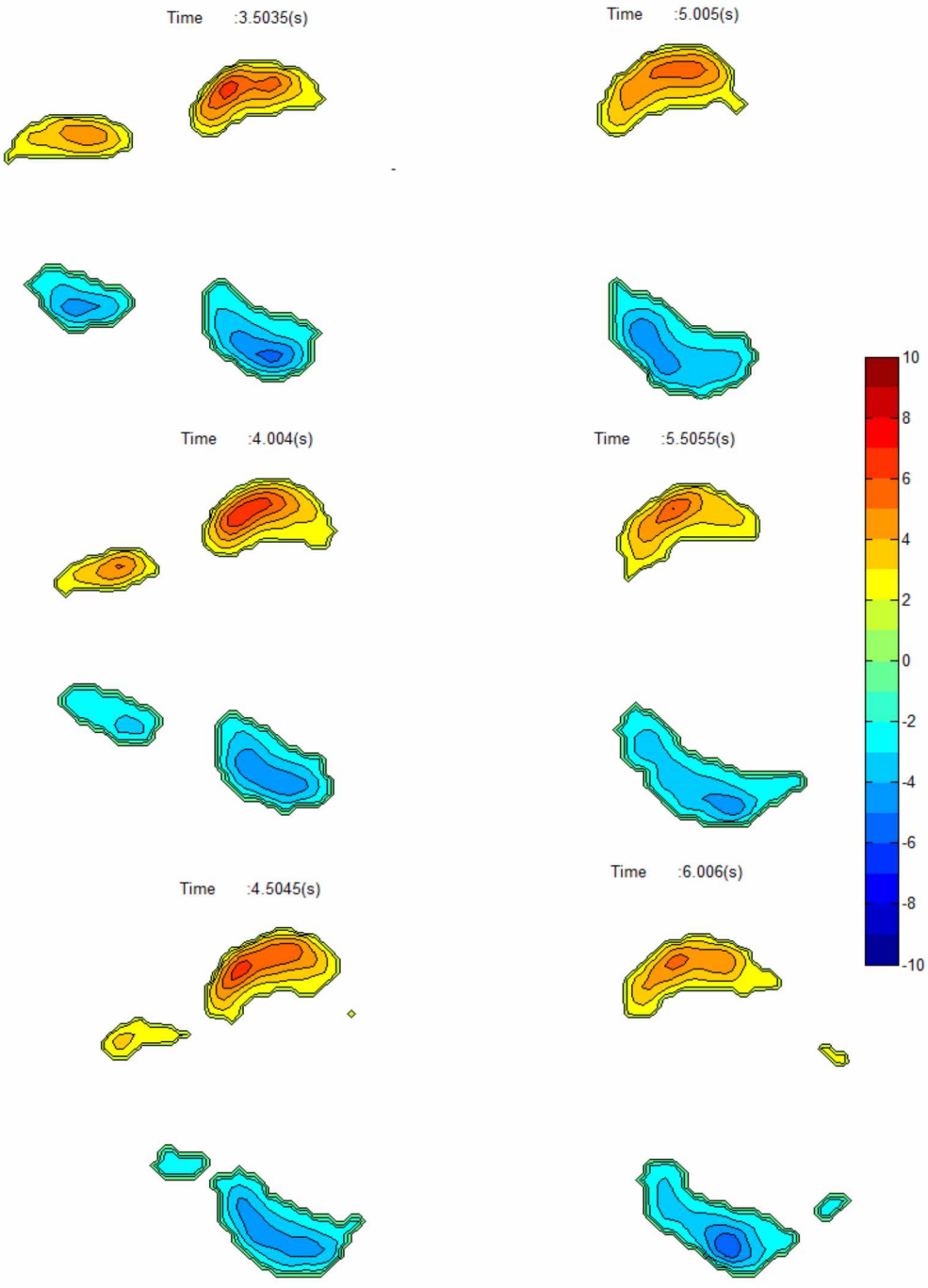

Figure 4.15 Vortex plot at Formation Time 2, Reynolds Number 5164, and SR_L 0.667

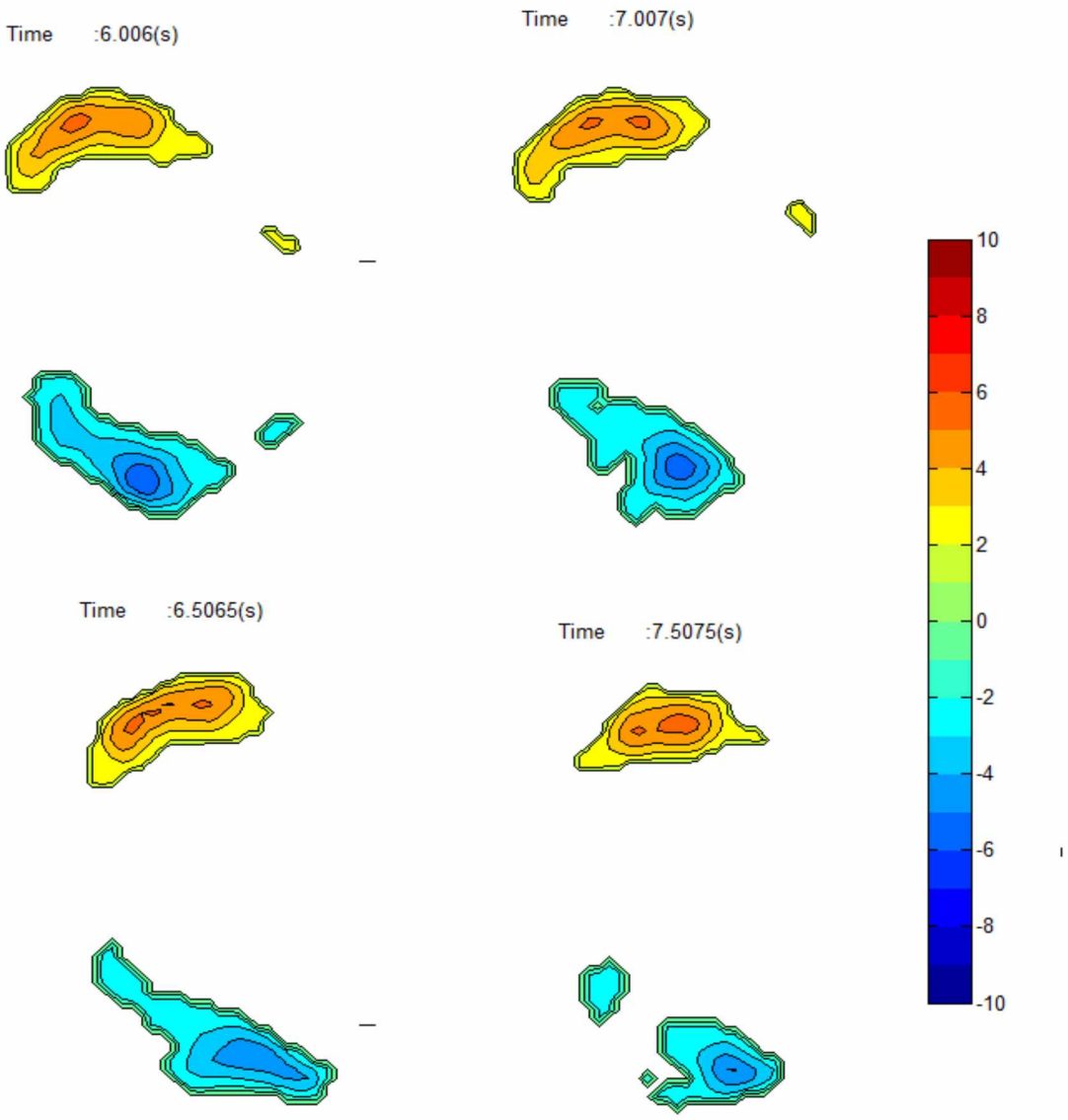

Figure 4.16 Vortex plot at Formation Time 2, Reynolds Number 5164, and SR_L 0.667

4.4.2 Trajectory of vortex rings

Figure 4.17 shows the trajectory of the vortex rings. The curve of Vortex Ring 1 shows the path of the leading ring and the curve of Vortex Ring 2 shows the path of the trailing ring in the interaction between the coaxial and co-rotating vortex rings. As can be observed, once the leading ring had fully developed, it began moving horizontally, and engaged in no vertical movement after full development. These results indicate that at Formation Time 2, the leading ring was the least affected by the trailing ring during the interaction between the coaxial and co-rotating vortex rings. Although the trailing ring initially began developing, it remained underdeveloped, and began moving not only horizontally and vertically but also downward, indicating that it was compressing. The trailing ring then attempted to come closer to the leading ring by moving upward toward its center until it ultimately began slowly merging with the leading ring.

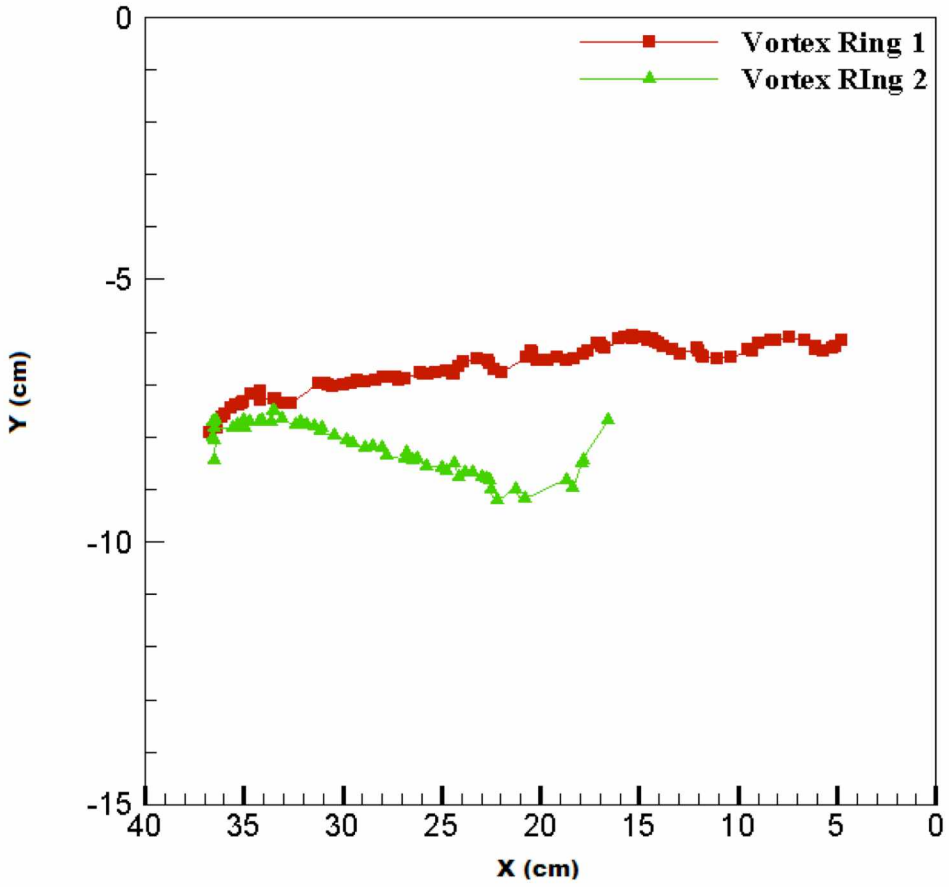

Figure 4.17 Vortex ring trajectory at Formation Time 2, Reynolds Number 5164, and SR_L 5164

4.4.3 Circulation at Formation Time 2

Figure 4.18 shows the circulation of the leading ring, trailing ring, dx, and dy of at Formation Time 2, Reynolds Number 5164, and SRL 0.476. As can be observed, the circulation of the leading ring increased during the development phase, after which it began decreasing as it attempted to stabilize its circulation. This attempt at stability is due to the high formation time, which increased the circulation above normal values. After the circulation of the ring had increased to a rate in accordance with its formation time, it began to decrease as the ring attempted to stabilize until eventually reaching a constant circulation. As the circulation of the trailing ring began decreasing, the circulation of the leading ring began increasing, indicating that the leading ring was absorbing some of the trailing ring's circulation to increase its circulation. Once the trailing ring had disappeared, the circulation of the leading ring began to decrease until reaching a normal level.

The dx curve provides information regarding the movement and distance between the vortex rings, while the dy curve provides information regarding the vertical distance between the rings. As can be observed from the dx curve, the distance between the rings decreased until they came sufficiently close to each other to merge. Although the dy curve generally remained constant, a slight increase occurred at the final stage as the trailing ring moved toward the center of the leading ring.

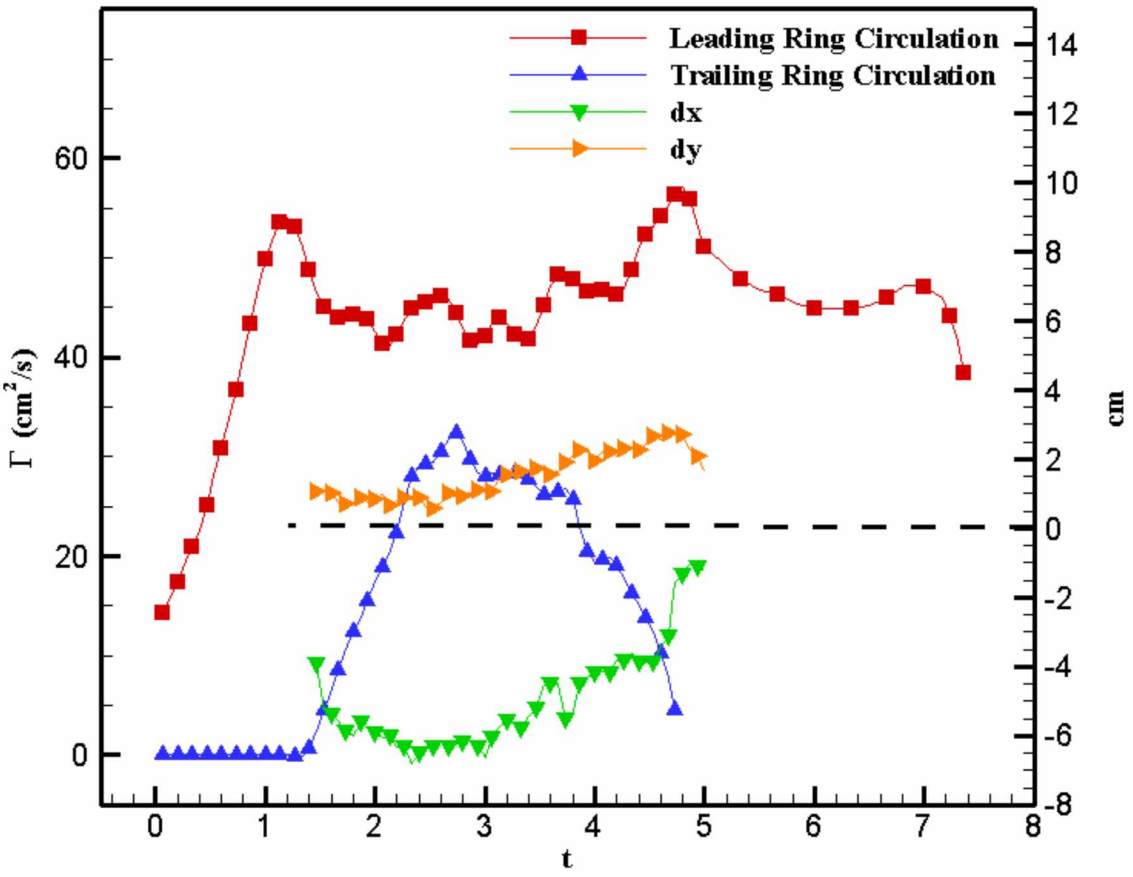

Figure 4.18 Vortex ring circulation at Formation Time 2

4.4.4 Reynolds Number

The Reynolds Number, which is directly proportional to the circulation of the vortex rings, and the non-dimensional frequency number are the most important parameters in the interaction between coaxial and co-rotating vortex rings. At Formation Time 2, the nature of this interaction was examined at Reynolds Numbers 5164, 7395, 8958, and 8977 and at different non-dimensional frequency numbers. The following section provides a detailed analysis of the results.

4.4.4.1 Reynolds Number 5164

Leading rings

Figure 4.19 shows the circulation of the leading rings at Formation Time 2, Reynolds Number 5164, and SR_L 0.769, 0.667, 0.588, 0.526, and 0.476. As can be observed, the circulation increased to a maximum point before decreasing until reaching a constant level with slight fluctuations, as well as that the path toward merging was shorter at lower non-dimensional frequency number numbers. An increase in leading ring circulation was observed at all non-dimensional frequency numbers, indicating that the leading ring was absorbing some of the circulation of the trailing ring.

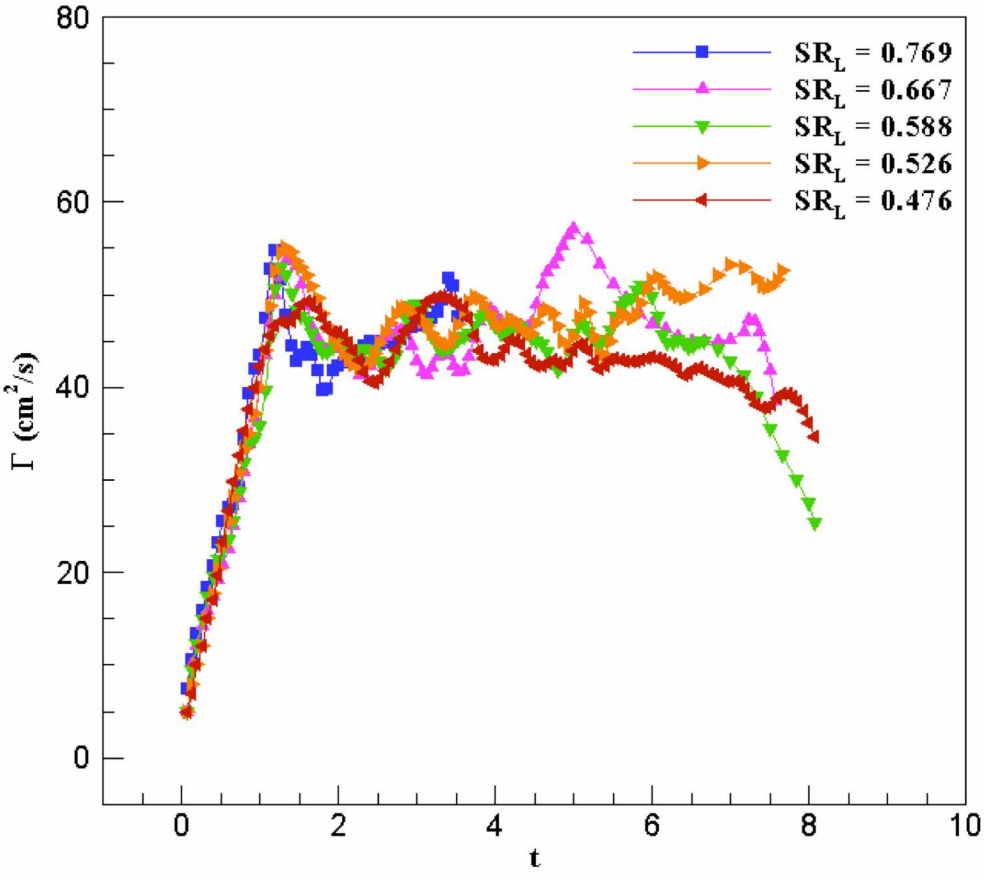

Figure 4.19 Leading ring circulation at Formation Time 2 and Reynolds Number 5164

Trailing rings

Figure 4.20 shows the circulation of the trailing rings at Formation Time 2, Reynolds Number 5164, and SR_L 0.769, 0.667, 0.588, 0.526, and 0.476. As can be observed, the rings followed the same pattern as had the rings at other Reynolds Numbers. As the non-dimensional frequency number increased, the gap between the

rings decreased, leading the rings to have a stronger interaction effect, which in turn caused the trailing ring to lose circulation.

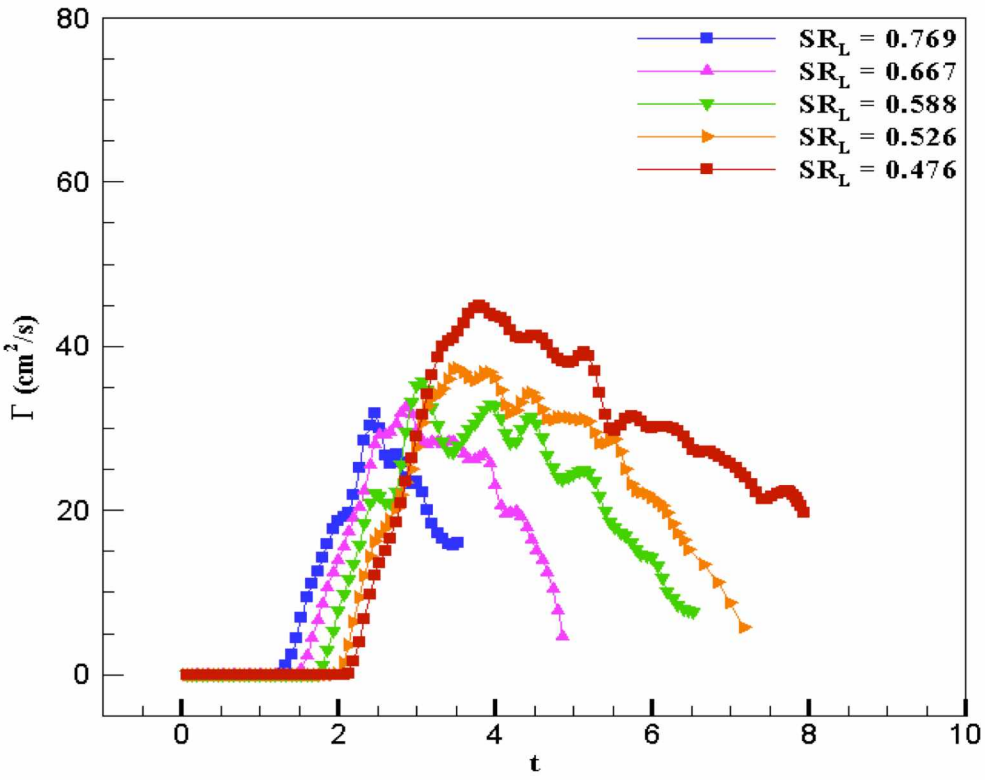

Figure 4.20 Trailing ring circulation at Formation Time 2 and Reynolds Number 5164

4.4.4.2 Reynolds Number 7395

Leading rings

Figure 4.21 shows the circulation at leading rings Formation Time 2, Reynolds Number 7395, and SR_L 0.739, 0.629, 0.548, and 0.485. At lower non-dimensional frequency numbers, an increase in circulation was observed after the rings had developed fully, the reason for which was explained in the previous section, whereas no increase in circulation was observed at higher non-dimensional frequency numbers.

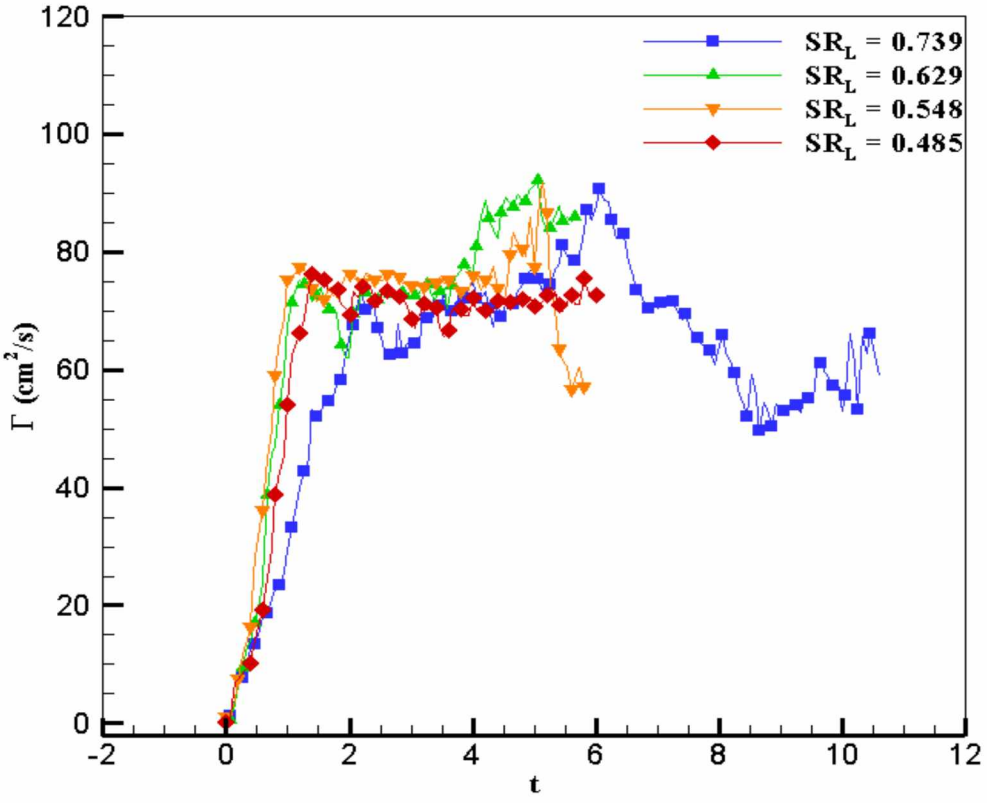

Figure 4.21 Leading ring circulation at Formation Time 2 and Reynolds Number 7395

Trailing rings

Figure 4.22 shows the circulation of the trailing rings at Formation Time 2, Reynolds Number 7395, and SR_L 0.739, 0.629, 0.548, and 0.485. As can be observed, the trailing ring at SR_L 0.73913 remained underdeveloped because it did not have sufficient time to develop, leading to a decrease in circulation. This result indicates that as the non-dimensional frequency number increases, the circulation decreases.

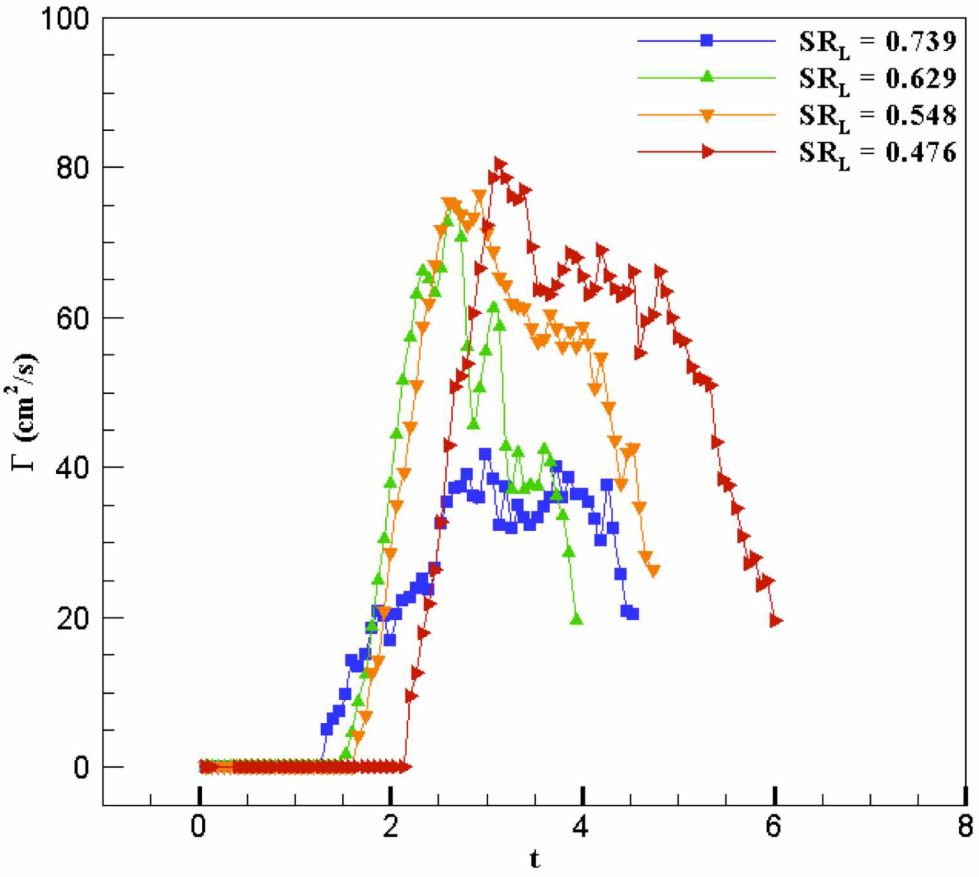

Figure 4.22 Trailing ring circulation at Formation Time 2 and Reynolds Number 7395

4.4.4.3 Reynolds Number 8958

Leading rings

Figure 4.23 shows the circulation of the leading rings at Formation Time 2, Reynolds Number 8958, and SR_L 0.714, 0.6, and 0.517. As can be observed, the circulation of the leading ring remained constant at lower non-dimensional frequency numbers but increased at higher non-dimensional frequency numbers. These results indicate that the leading ring absorbs circulation from the trailing ring at higher non-dimensional frequency numbers, which explains the variations in circulation observed for the rings at SR_L 0.714.

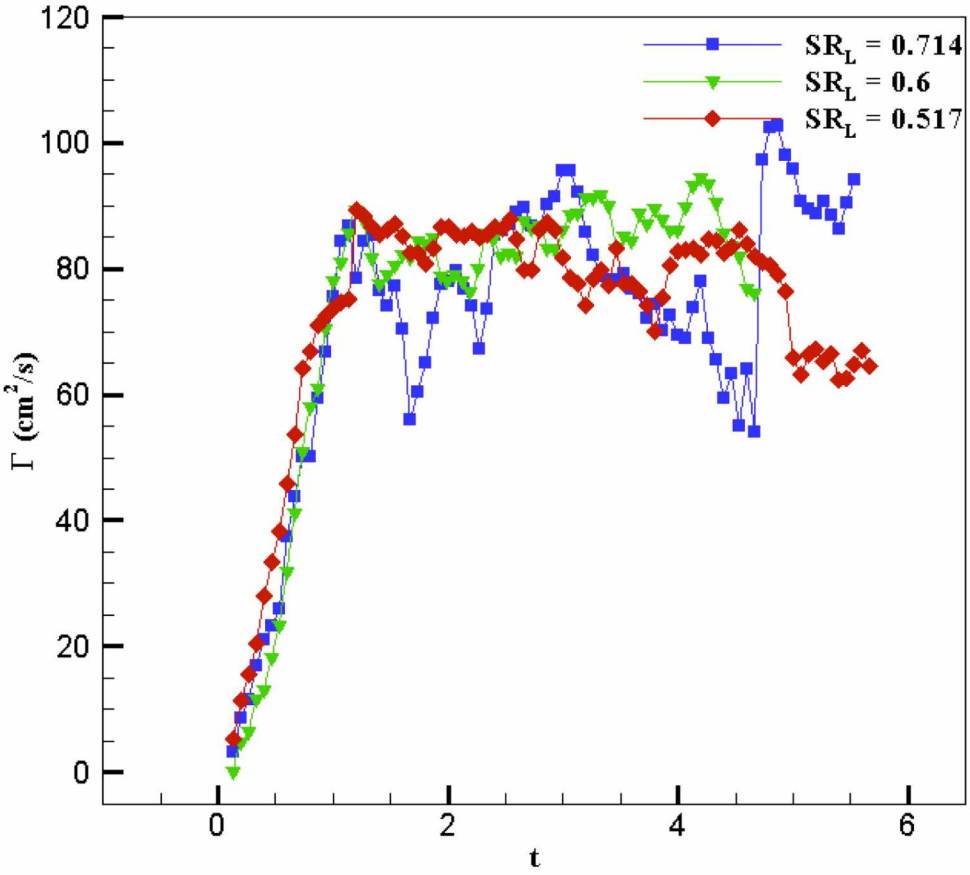

Figure 4.23 Leading ring circulation at Formation Time 2 and Reynolds Number 8958

Trailing rings

Figure 4.24 shows the circulation of the trailing rings at Formation Time 2, Reynolds Number 8958, and SR_L 0.714, 0.6, and 0.517. As can be observed, the rings displayed a trend similar to that of the rings at other Reynolds Numbers; that is, as the non-dimensional frequency number increased, the circulation decreased. However, the rings at this Reynolds Number differed from those in previous experiments in that the

rings at Reynolds Number 8958 fully developed, even at low non-dimensional frequency numbers. The reason for this difference is that the leading ring could fully develop and move forward, and it thus had no effect on the circulation of the trailing ring. Therefore, the only phenomenon that caused the rings to lose circulation at Reynolds Number 8958 was vortex shedding.

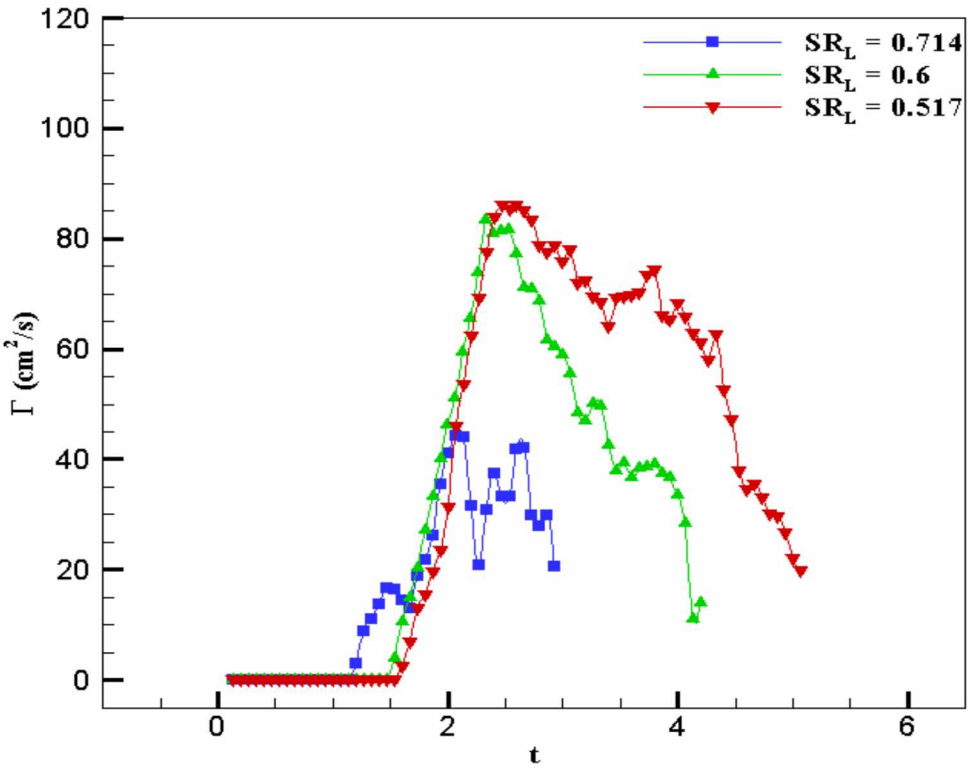

Figure 4. 24 Trailing ring circulation at Formation Time 2 and Reynolds Number 8958

4.4.4.4 Reynolds Number 8977

Leading rings

Figure 4.25 shows the circulation of the leading rings at Formation Time 2, Reynolds Number 8977, and SR_L 0.666, 0.545, and 0.461. As can be observed, the rings followed the same trend as had the rings at Reynolds Number 5164, 7395, and 8957 that of an increase in the circulation of the leading rings at higher non-dimensional frequency numbers (SR_L 0.666 and 0.545). Despite some fluctuations, the circulation of the leading ring generally remained constant at SR_L 0.461.

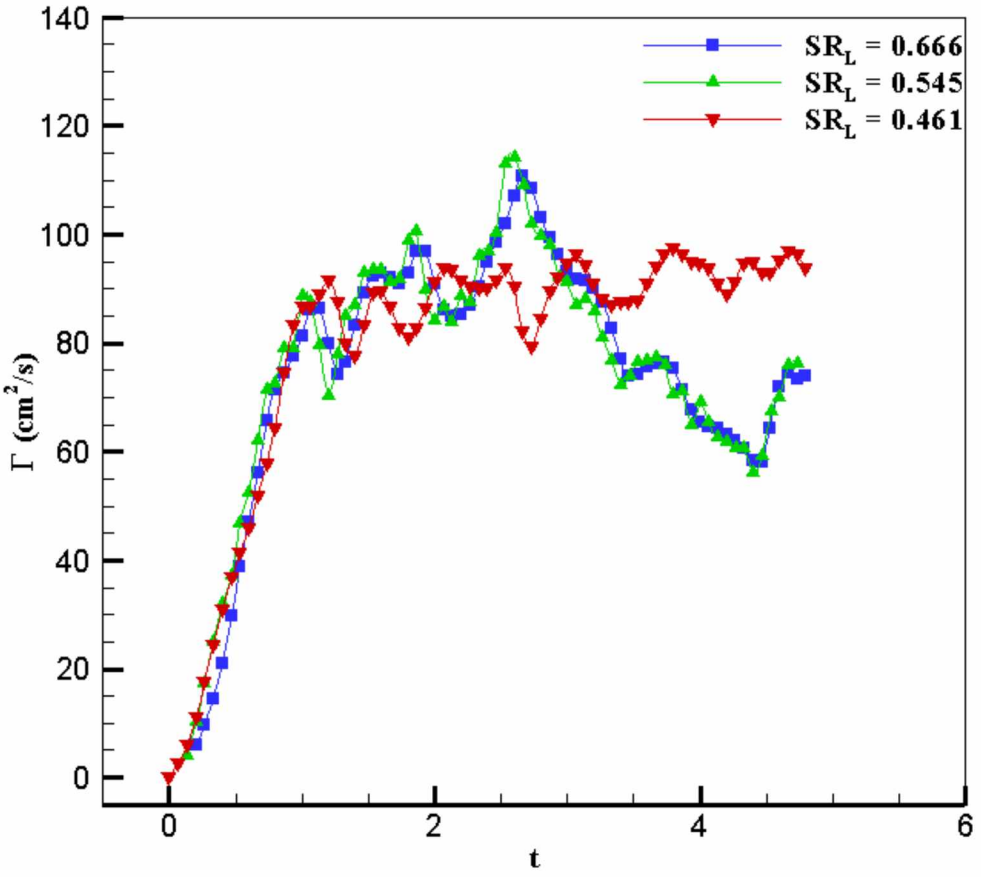

Figure 4.25 Leading ring circulation at Formation Time 2 and Reynolds Number 8977

Trailing rings

Figure 4.26 shows circulation of the trailing rings at Formation Time 2, Reynolds Number 8977, and SR_L 0.666, 0.629, and 0.548. As can be observed, although the leading ring could fully develop and begin to move relatively rapidly at SR_L 0.629 and 0548, the trailing ring could not fully develop at these low non-dimensional frequency

numbers. As the trailing ring could not fully develop at SR_L 0.548, there was no interaction between the rings, leading to the peak in circulation observed in the plot.

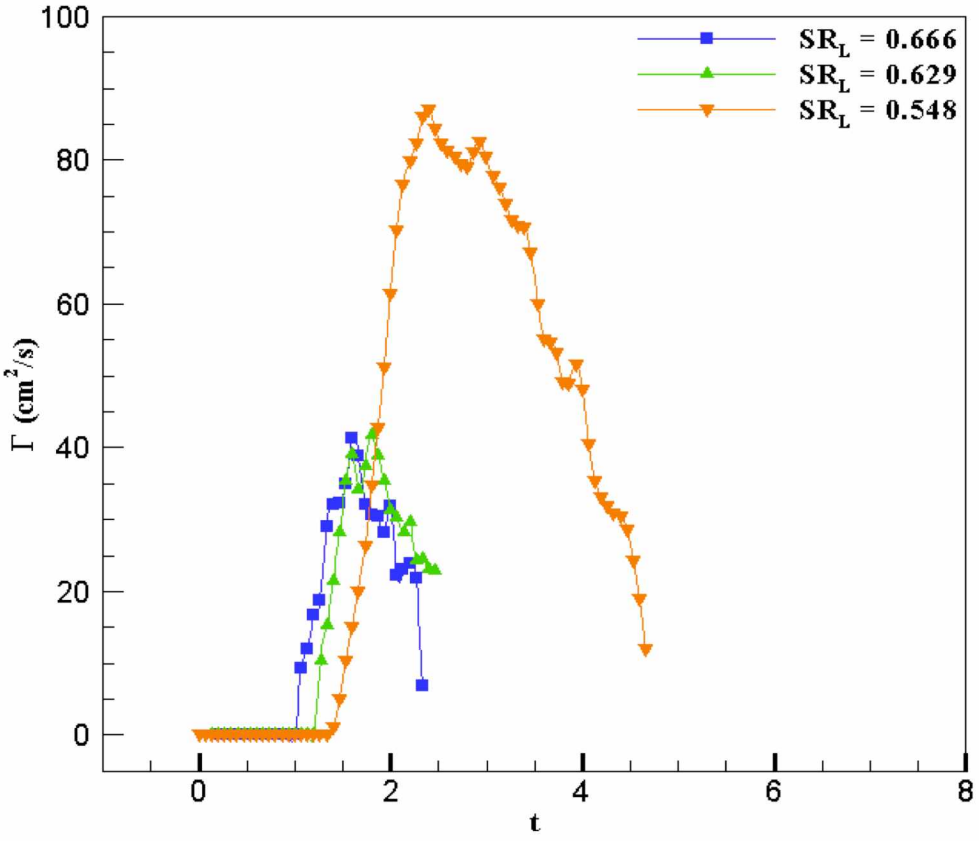

Figure 4.26 Trailing ring circulation at Formation Time 2 and Reynolds Number 8977

4.5 Formation Time 3

4.5.1 Vortex plot

Figures 4.27, 4.28 and 4.29 shows the plots for the interaction of the vortex rings at Formation Time 3 with the time step in the interaction of the vortex rings listed above each plot. As can be observed, development of the leading ring occurred at Time Steps 0.5 to 2 seconds and development of the trailing ring at Time Steps 2.5 to 4 seconds. At Time Steps 4 to 5.5 seconds, the trailing ring lost circulation in the form of shedding vorticity, leading to the appearance of a third vortex ring behind the trailing ring. Thus, two separate vortex rings were observed at Time Steps 6 to 7 seconds, as the shredded vortex ring had disappeared into the surrounding fluid. These two rings did not directly interact with each other. After Time Step 7 seconds, a decrease in the vortex levels of the rings was observed. No elongation in rings was observed in this set of experiments. These results indicate that the circulation of the leading ring remained constant and did not absorb any circulation from the trailing ring, while the trailing ring lost much of its circulation through strong shedding of vorticity until it eventually disappeared.

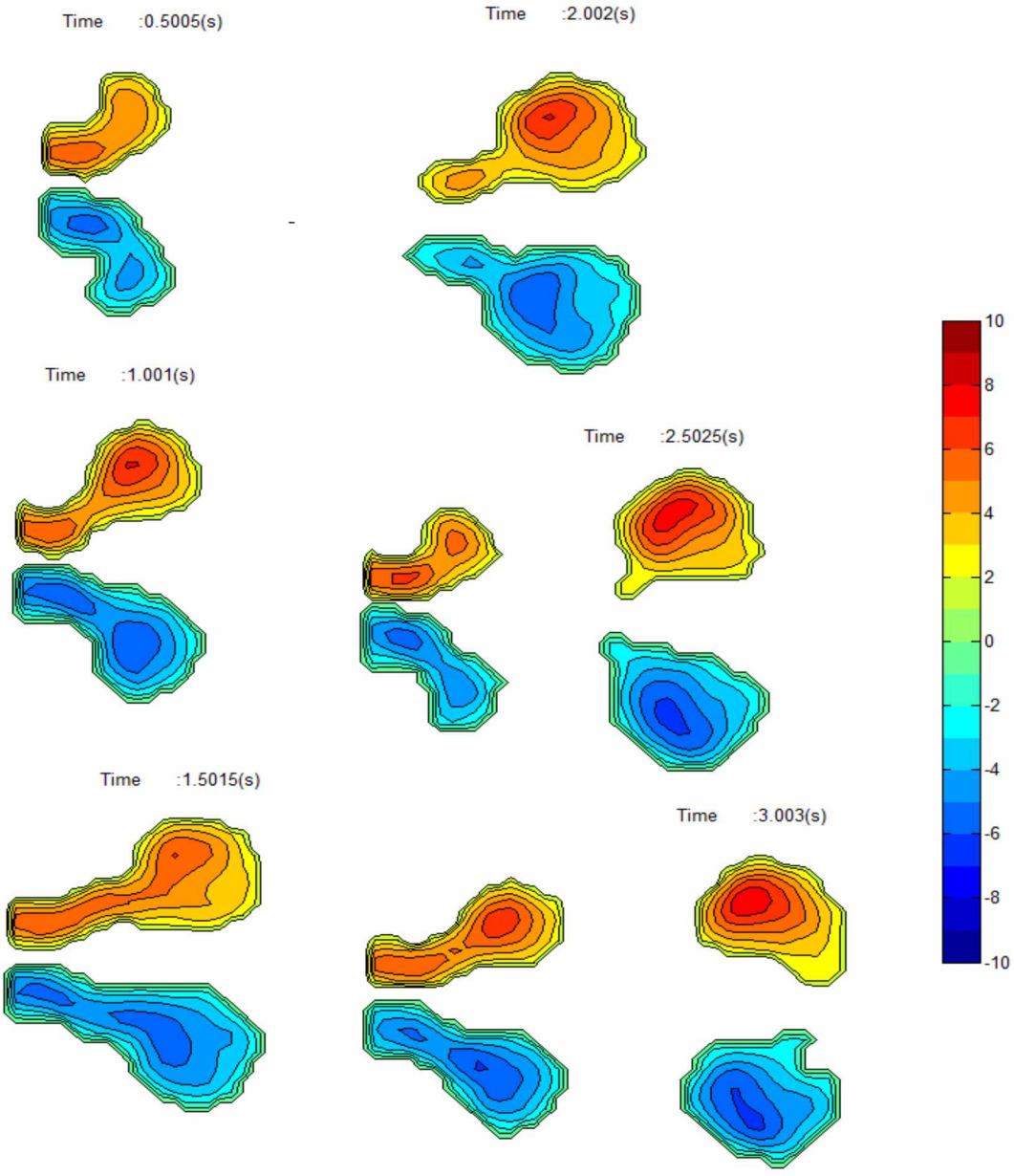

Figure 4.27 Vortex plot of vortex ring interaction at Formation Time 3, Reynolds Number 9012, and SR_L 0.75

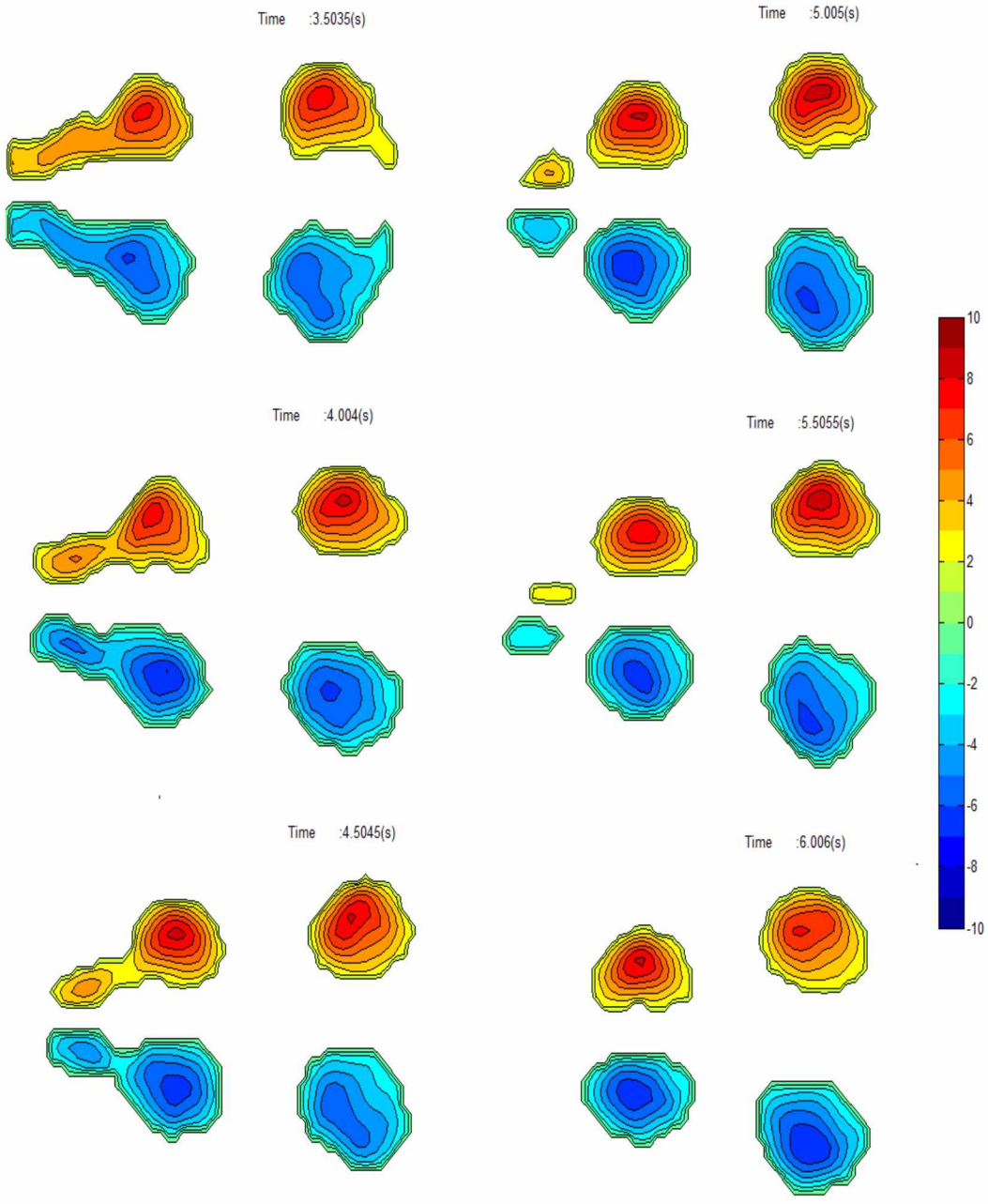

Figure 4.28 Vortex plot of vortex ring interaction at Formation Time 3, Reynolds Number 9012, and SR_L 0.75

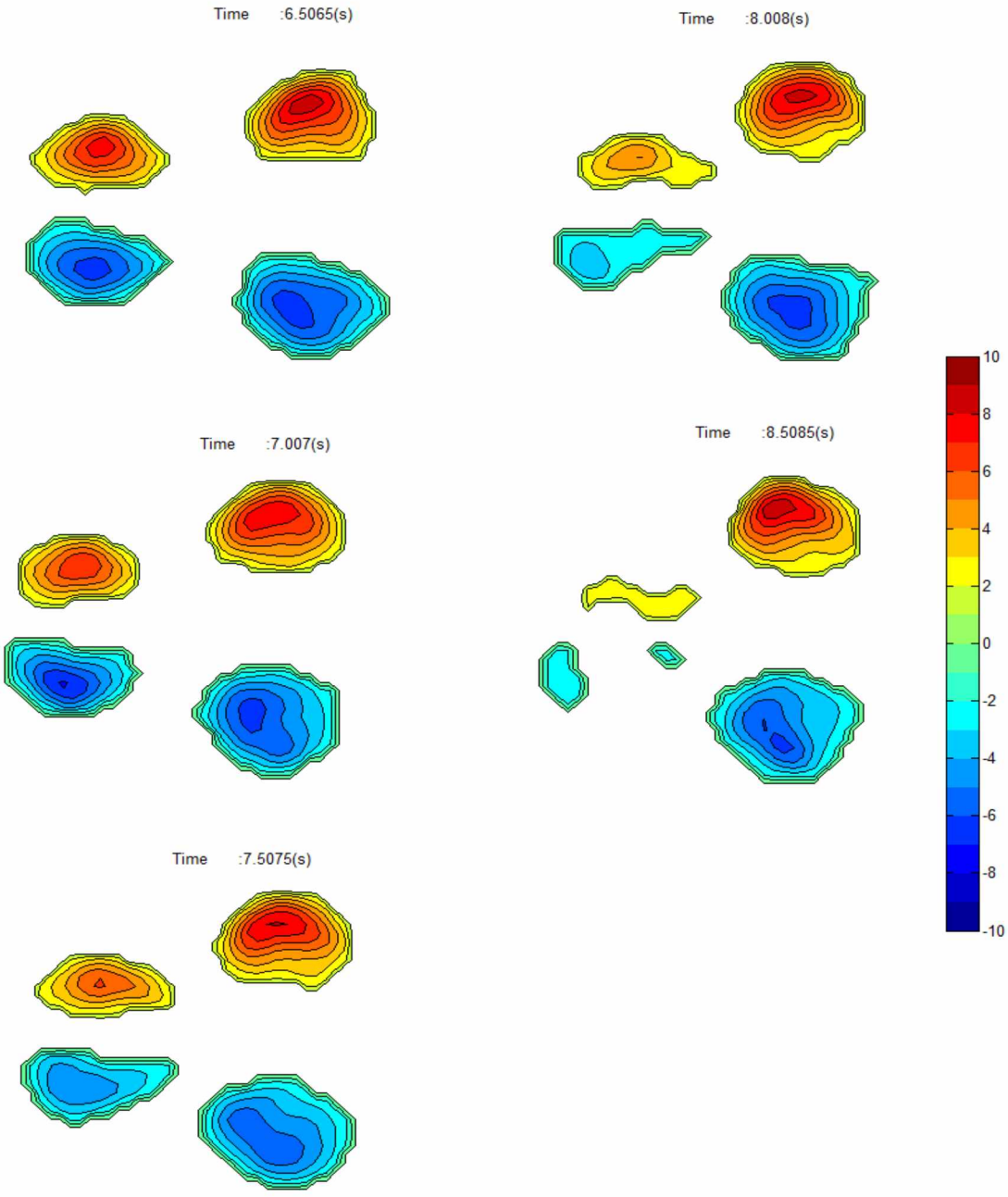

Figure 4.29 Vortex plot of vortex ring interaction at Formation Time 3, Reynolds Number 9012, and SR_L 0.75

4.5.2 Trajectory of vortex rings

Figure 4.30 shows the trajectory of the vortex rings. The curve of Vortex Ring 1 shows the path of the leading ring and the curve of Vortex Ring 2 shows the path of the trailing ring. As can be observed, both rings began forming at the same point. The movement of the leading ring, which was less affected by the interaction than the trailing ring, was the same as that of the leading ring at Formation Time 2. In contrast, the movement of the trailing ring, which moved downward before disappearing, differs from that of the trailing ring at Formation Times 1.5 and 2.

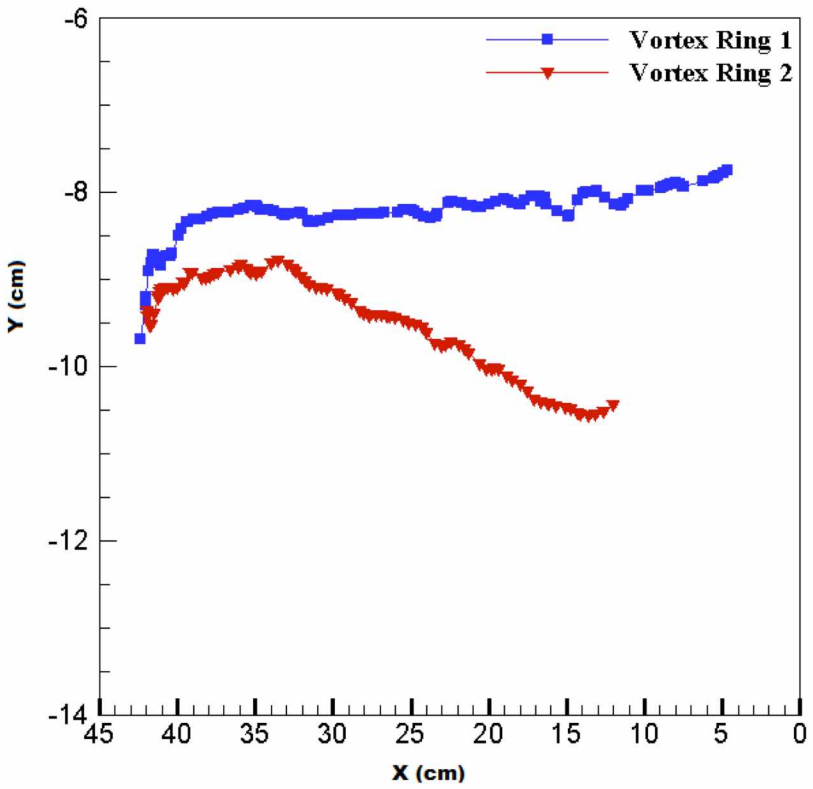

Figure 4.30 Vortex ring trajectory at Formation Time 3, Reynolds Number 9012, and SR_L 0.937

4.5.3 Circulation at Formation Time 3

Figure 4.31 shows the circulation of the interaction of the vortex rings at Formation Time 3, with the curves of the circulation of the leading ring and trailing ring labeled dx and dy, respectively. As can be observed, the rings followed a similar trend as that shown in the vorticity plot. The leading ring was less affected by the trailing ring, which behaved as a separate single vortex ring and in which all three stages of the development of a single vortex ring can be observed. This pattern was not observed for the trailing ring at Formation Times 1.5 and 2. These results indicate that the trailing ring decayed without the interference of outside factors, and not because of its direct interaction with the leading ring.

Analysis of the dx curve, which provides information regarding the horizontal movement and distance between the rings, indicates that the distance between the rings decreased as the rings passed on, leading the rings to come closer together. This result supports the analysis made by the vortex plot. The dy curve, which provides information regarding the vertical movement and distance between the rings, generally remained constant before slightly increasing at the final stage, indicating that the trailing ring began moving toward the center of the leading ring, which increased the dy between the vortex rings.

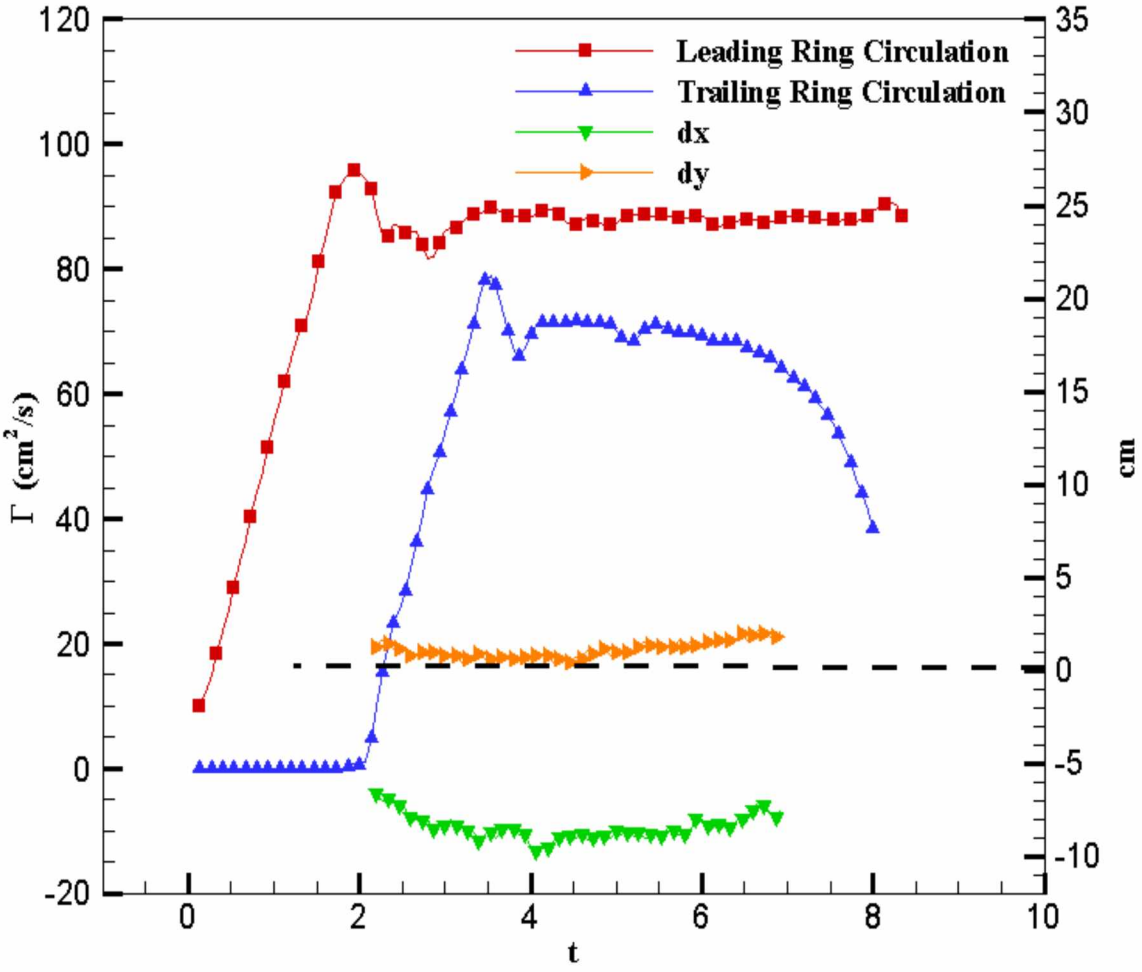

Figure 4.31 Vortex ring circulation at Formation Time 3, Reynolds Number 9012, and SR_L 0.937

4.5.4 Reynolds Number

At Formation Time 3, a series of experiments at Reynolds Numbers 9012, 10971, 10734, and 10583 were conducted at several non-dimensional frequency numbers. The results of the experiments and a detailed analysis thereof are reported in the following sections

4.5.4.1 Reynolds Number 9012

Leading rings

Figure 4.32 shows the circulation of the leading rings at Formation Time 3, Reynolds Number 9012, and SR_L 0.937, 0.8823, 0.833, 0.789, and 0.75. As can be observed, the circulation of the leading ring generally remained constant, irrespective of the non-dimensional frequency number, indicating that it was not affected by the circulation of the trailing ring.

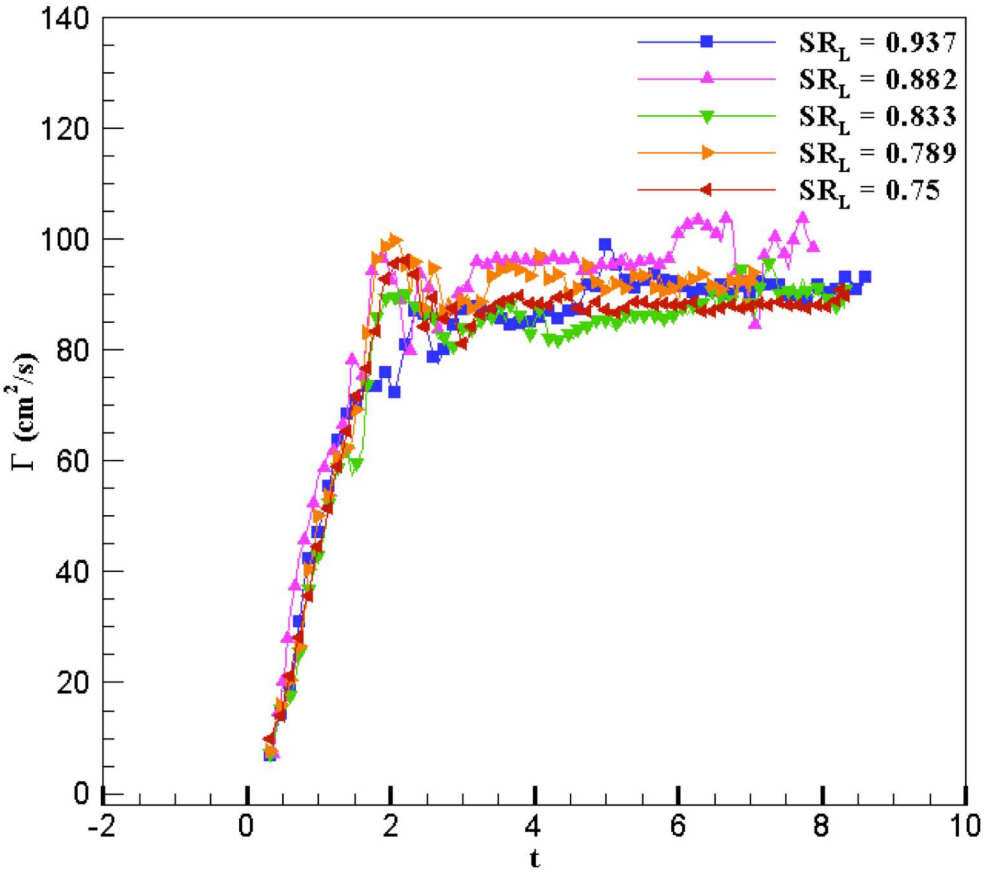

Figure 4.32 Leading ring circulation at Formation Time 3 and Reynolds Number 9012

Trailing rings

Figure 4.33 shows the circulation of the trailing ring at Formation Time 3, Reynolds Number 9012, and SR_L 0.937, 0.8823, 0.833, 0.789, and 0.75. As can be observed, the circulation of the trailing ring increased as the non-dimensional frequency

number decreased. This result, combined with observation that the rate of decrease in circulation was lower at higher non-dimensional frequency numbers at Formation Time 3 compared to the rate of decrease at Formation Times 1.5 and 2, indicates that the leading ring was moving at a sufficiently rapid rate so as to have no effect on the trailing ring, despite the small gap between their formation times.

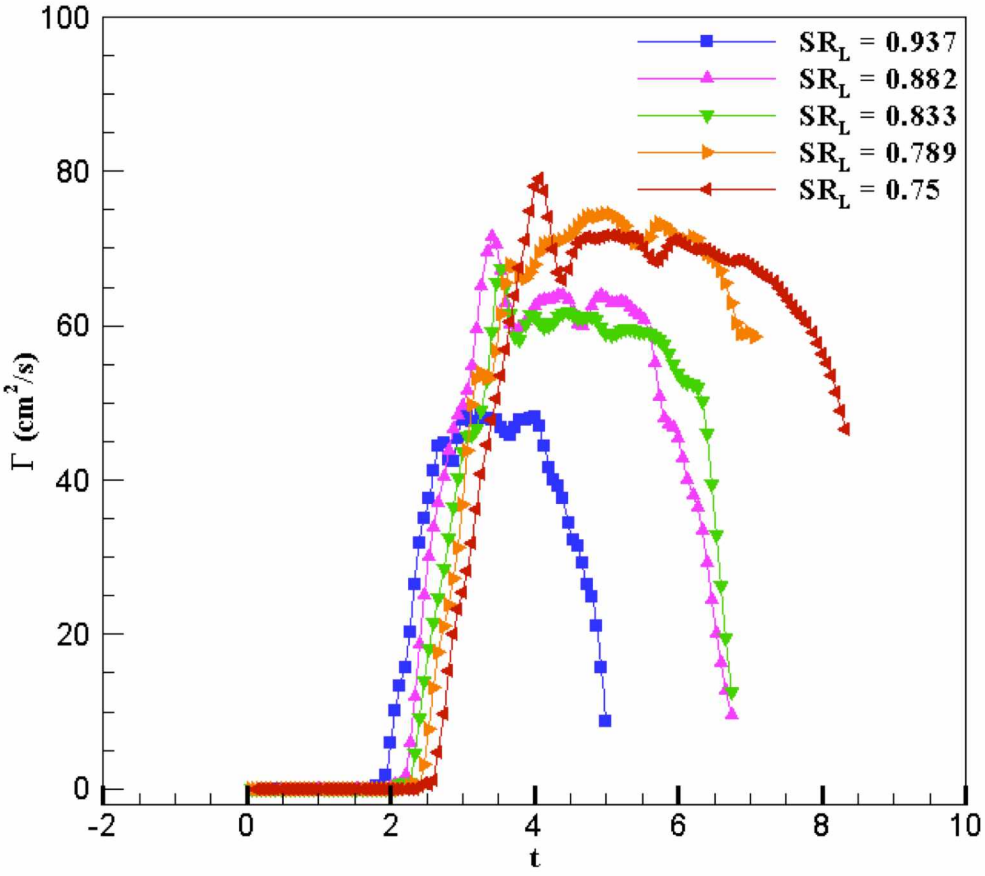

Figure 4. 33 Trailing ring circulation at Formation Time 3 and Reynolds Number 9012

4.5.4.2 Reynolds Number 10583

Leading rings

Figure 4.34 shows the circulation of the leading rings at Formation Time 3, Reynolds Number 10583, and SR_L 0.90476, 0.826, 0.76, 0.70, and 0.655. As can be observed, the rings followed a pattern similar to that observed for the rings at Reynolds Number 9012, while also displaying a turbulent nature that caused fluctuations in circulation.

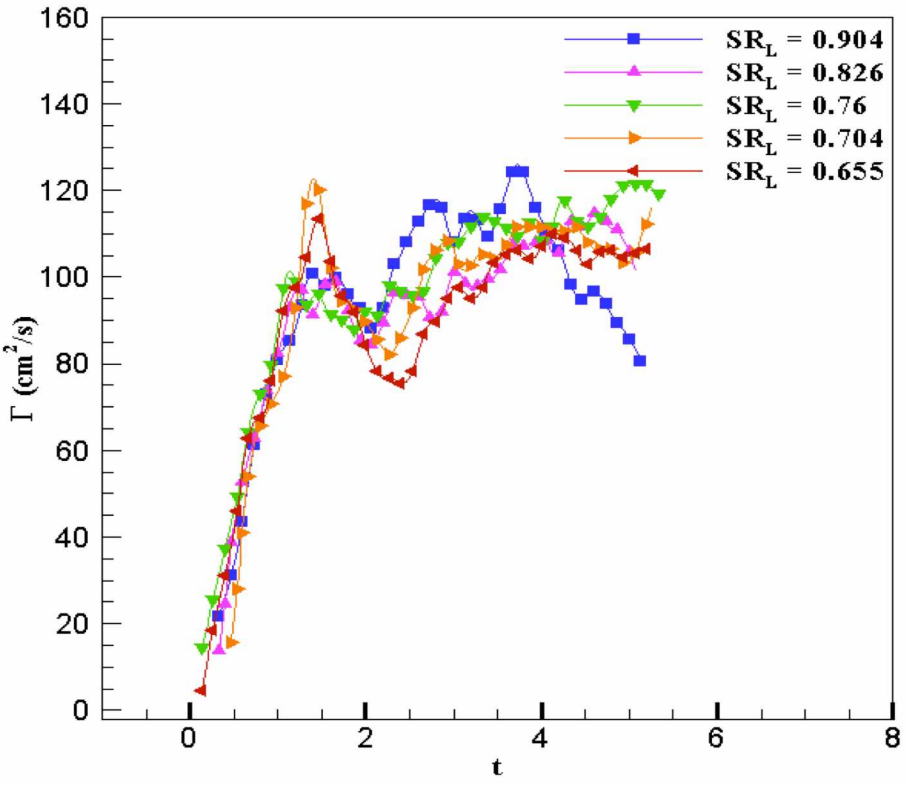

Figure 4.34 Leading ring circulation at Formation Time 3 and Reynolds Number 10583

Trailing rings

Figure 4.35 shows the circulation of the trailing rings at Formation Time 3, Reynolds Number 10583, and SR_L 0.90476, 0.826, 0.76, 0.703, and 0.655. As can be observed, the rings followed a pattern similar to that observed for the rings at Reynolds Numbers 9012 and 10583, with the circulation of the trailing ring increasing as the non-dimensional frequency number decreased.

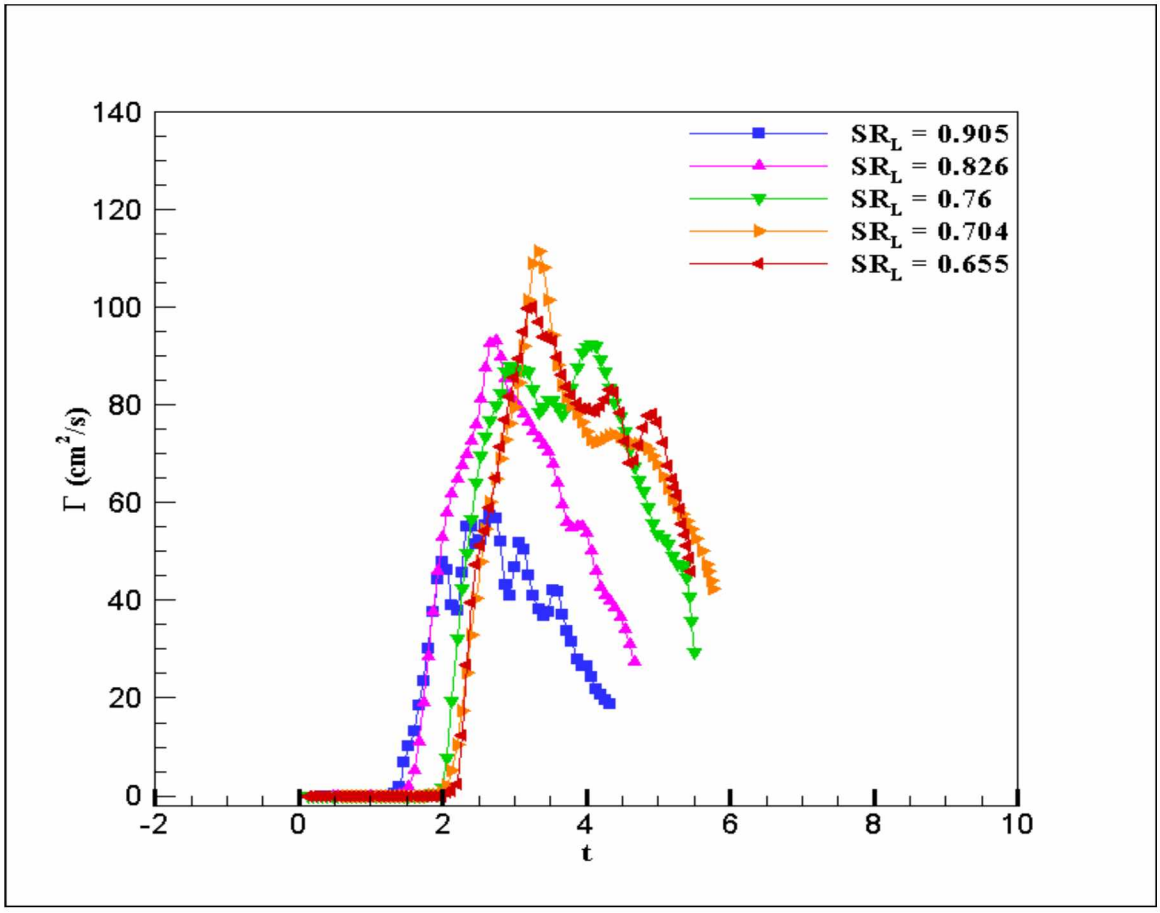

Figure 4.35 Trailing ring circulation at Formation Time 3 and Reynolds Number 10583

4.5.4.3 Reynolds Number 10734

Leading rings

Figure 4.36 shows the circulation of the leading rings at Formation Time 3, Reynolds Number 10734, and SR_L 0.917, 0.846, 0.785, 0.733, and 0.687. As can be observed, despite some uncertainty due to the turbulent nature of the vortex rings, the circulation of the curves generally remained constant.

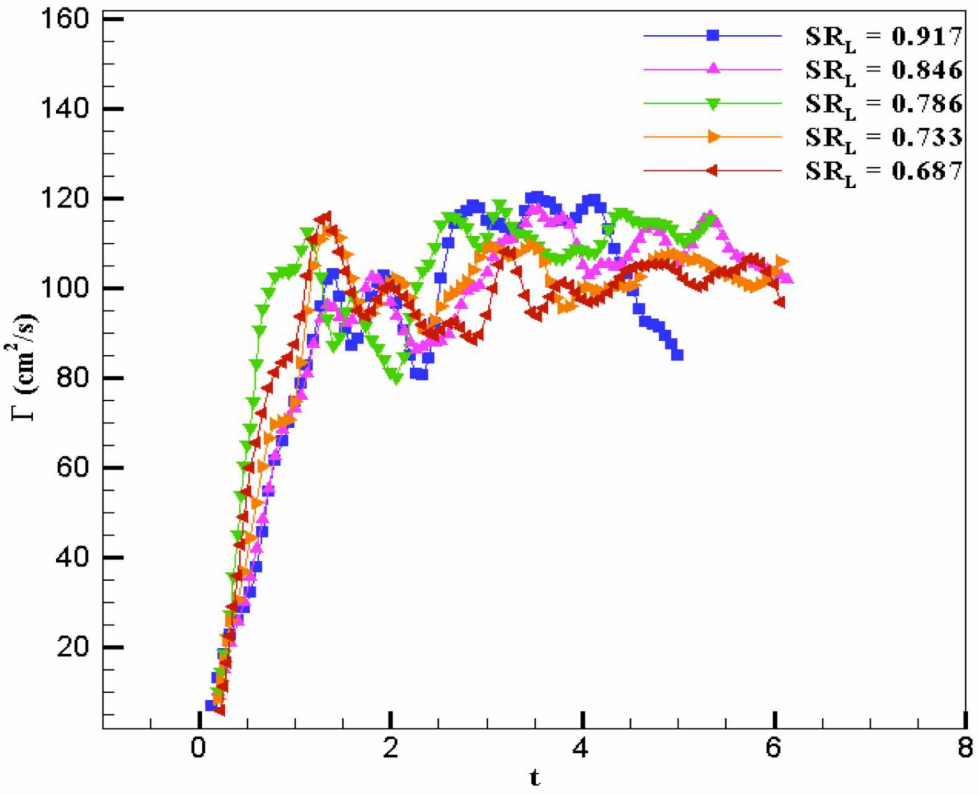

Figure 4.36 Leading ring circulation at Formation Time 3 and Reynolds Number 10734

Trailing rings

Figure 4.37 shows the circulation of the trailing rings at Formation Time 3, Reynolds Number 10734, and SR_L 0.917, 0.846, 0.785, 0.733, and 0.687. As can be observed, the rings displayed a pattern similar to that observed for the rings at Reynolds Numbers 9012, 10583, and 10734, with the circulation of the trailing ring increasing as the non-dimensional frequency number decreased.

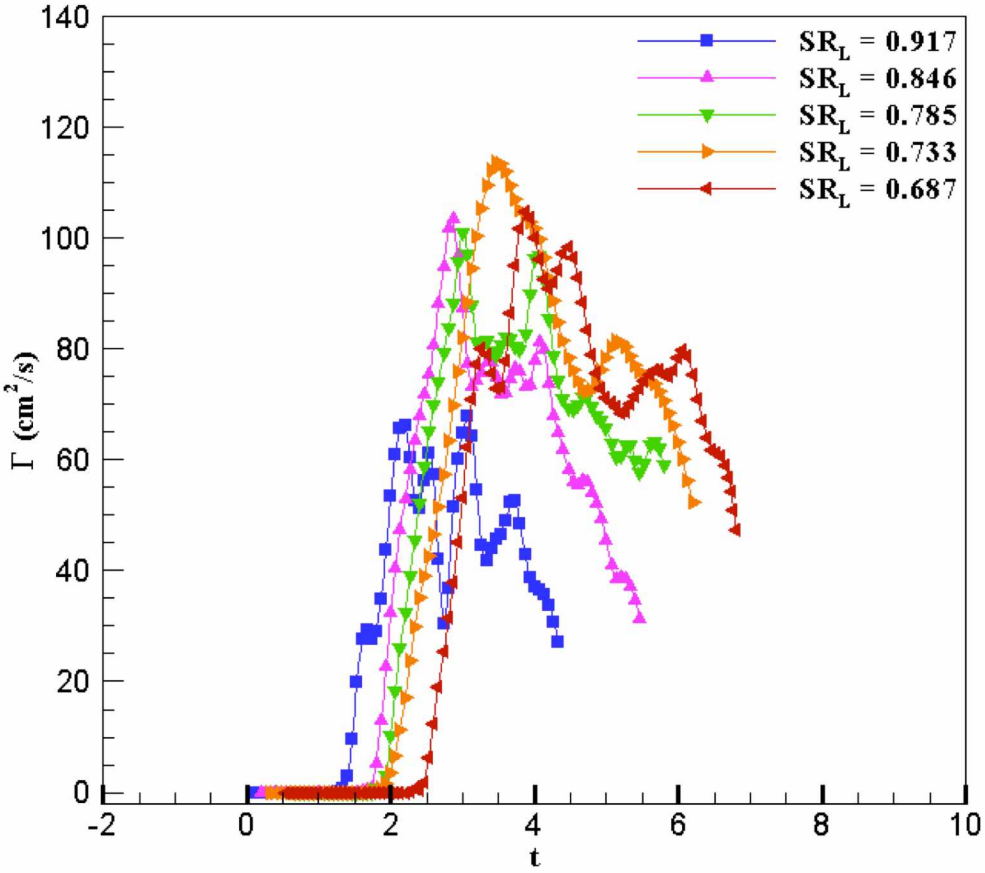

Figure 4.37 Trailing ring circulation at Formation Time 3 and Reynolds Number 10734

4.5.4.4 Reynolds Number 10971

Leading rings

Figure 4.38 shows the circulation of the leading rings at Formation Time 3, Reynolds Number 10971, and SR_L 0.928, 0.867, 0.812, 0.764, and 0.722. As can be observed, the circulation of the leading rings displayed some uncertainty due to the high Reynolds Number, as the circulation of vortex rings becomes turbulent at high Reynolds Numbers. The circulation of the leading ring remained constant, which indicates that it was less affected by the trailing ring.

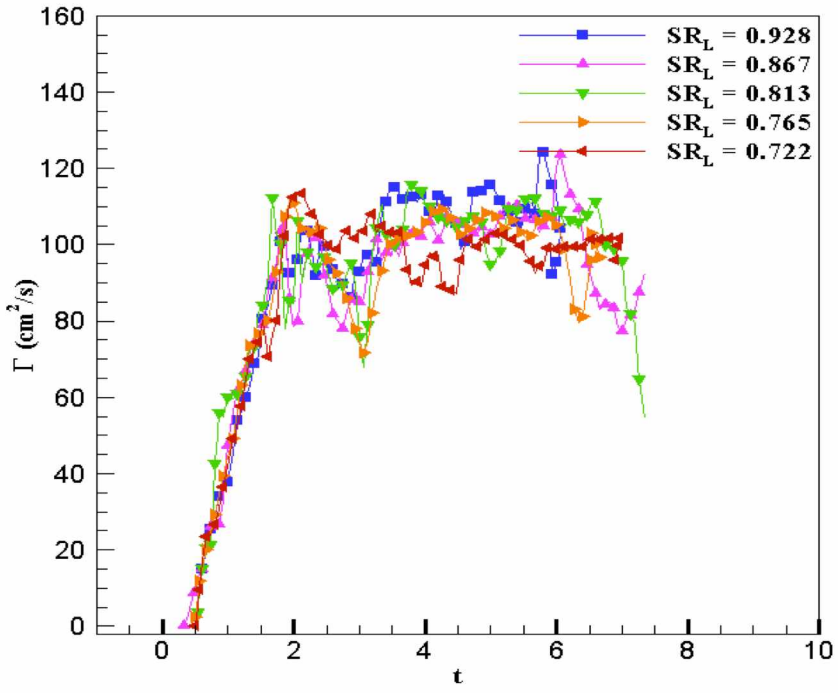

Figure 4.38 Leading ring circulation at Formation Time 3 and Reynolds Number 10971

Trailing ring circulation

Figure 4.34 shows the circulation of the trailing rings at Formation Time 3, Reynolds Number 10971, and SR_L 0.928, 0.867, 0.812, 0.764, and 0.722. As can be observed, the maximum circulation of the trailing ring increased with a decrease in the non-dimensional frequency number due to the turbulent nature of the vortex rings.

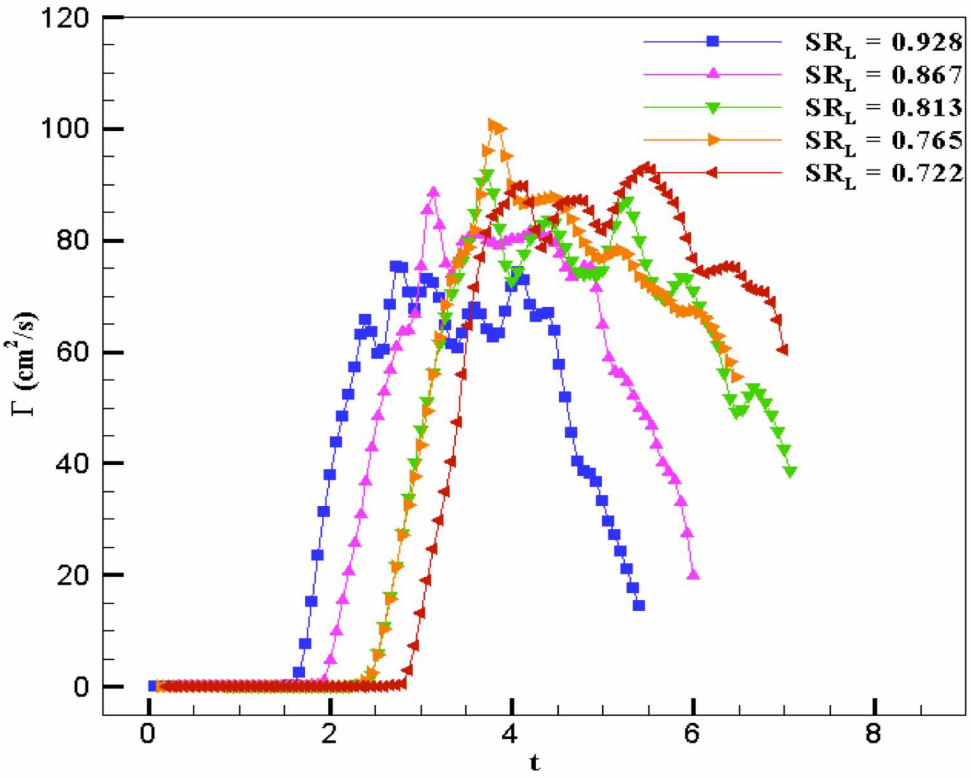

Figure 4.39 Trailing ring circulation at Formation Time 3 and Reynolds Number 10971

Chapter 5 Conclusion

The goal of this study was to investigate the role of formation time, Reynolds Number, and non-dimensional frequency number, the three most significant parameters in the dynamics of vortex rings, in the interaction between the co-axial and co-rotating rings. To generate and investigate vortex rings with the required characteristics, a series of experiments were conducted at Formation Times 1.5, 2, and 3, with the experiments at each formation time repeated at different Reynolds Numbers, and the experiments at each Reynolds Number in turn repeated at different non-dimensional frequency numbers. After data collection, DPIV analysis of the results was performed to quantitatively characterize the trajectory and circulation of the rings.

Formation Time 1.5

Analysis of the trajectory plot at Formation Time 1.5 indicates that the rings had attempted to undergo leapfrogging, which was observed between rings at low Reynolds Numbers and high non-dimensional frequency numbers. Examination of the trajectory of the rings also reveals that the trailing ring had been compressing and moving toward the center of the leading ring while the leading ring had been expanding. After undergoing leapfrogging, the rings changed position, and then repeated the expansion and compression process until undergoing leapfrogging a second time. At Formation Time 1.5, Reynolds Number 2836, and SR_L 0.769, the rings underwent leapfrogging two times before merging after completing the second leapfrogging cycle. At high Reynolds

Numbers and low non-dimensional frequency numbers, the rings attempted to undergo leapfrogging, but were not able to complete the leapfrogging cycle.

The rings that were able to undergo leapfrogging displayed a circulation pattern different from that of the rings that were not able to undergo leapfrogging. For the former, the circulation of the trailing ring decreased while the circulation of the leading ring increased until the trailing ring reached the center of the leading ring, at which point the rings underwent leapfrogging. After the trailing ring had passed through the center of the leading ring, the circulation of the trailing ring began increasing while the circulation of the leading ring began decreasing, and they continued to increase and decrease until undergoing leapfrogging for a second time. At the same time, the rings were experiencing a loss in circulation that caused them to merge after completing the second leapfrogging cycle.

Those rings that unsuccessfully attempted to undergo leapfrogging were not able to complete a leapfrog cycle due to the loss of circulation in the trailing ring, which increased as the Reynolds Number increased. In contrast, the circulation of the leading ring remained constant for all the rings that could not undergo leapfrogging. These results indicate that as the non-dimensional frequency numbers decreases, the tendency to undergo leapfrogging decreases. Observation of a high loss in the circulation of the trailing ring at high non-dimensional frequency numbers indicates that the rings are close to each other at these numbers, allowing the leading ring to have a strong effect on the trailing ring. At Formation Time 1.5, the velocity of the rings at all Reynolds Numbers

and at all non-dimensional frequency numbers tested was low, allowing for interaction between the rings in all experiments conducted at Formation Time 1.5.

Formation Time 2

Observation of the trajectory plot at Formation Time 2 reveals that the rings did not undergo leapfrogging, and that while the leading ring remained constant over time, the trailing ring compressed and moved toward the center of the leading ring before finally merging with it. Unlike the behavior of the rings at Formation Time 1.5, the behavior of the rings at Formation Time 2 was not the same at all Reynolds Numbers. At low Reynolds Numbers, a strong interaction was observed between the rings. While a strong interaction was observed between the rings at Reynolds Number 5164 at all non-dimensional frequency numbers, a strong interaction was observed between the rings at Reynolds Number 7395 at only SR_L 0.485. The other rings have least effect due to interaction. As the Reynolds Number increases, the same trend was observed. The reason for this phenomenon is that at low non-dimensional frequency numbers, the leading ring gains velocity, leading it to move away from the trailing ring. Thus, as the non-dimensional frequency number increases, the circulation loss of the rings increases.

Formation Time 3

The trajectory plot of the rings at Formation Time 3 shows that the rings interacted with each other, with the rings at the lowest non-dimensional frequency number showing the strongest interaction, and were turbulent in nature. While the circulation of the leading ring, which underwent no major change in its path, remained constant, similar to that of

the leading ring at Formation Time 2, the trailing ring compressed until finally disappearing into the surrounding fluid. As the non-dimensional frequency number increased, the leading ring began moving faster compared to its velocity at Formation time 2 at the same non-dimensional frequency number, leading to an increase in the vortex shedding rate. As the non-dimensional frequency number decreased, the gap between the rings increased, leaving the trailing ring unable to come closer to the leading ring.

Chapter 6 References

Batchelor, G. K. (1967). An Introduction to Fluid Mechanics, Cambridge University Press.

Dabiri, J. O. and M. Gharib (2004). "Fluid Entrainment by Isolated Vortex Rings." Journal of Fluid Mechanics 511: 311-31.

Dabiri, J. O. and M. Gharib (2005). "The role of optimal vortex formation in biological fluid transport." Proceedings of the Royal society B: Biological Sciences 272(1572): 1557-1560.

Gharib, M., E. Rambod, A. Kheradvar, D. J. Sahn, and J. O. Dabiri (2006). "Optimal vortex formation as an index of cardiac health." Proceedings of the National Academy of Sciences 103(16): 6305-6308.

Gharib, M., E. Rambod, K. Shariff (1998). "A universal time scale for vortex ring formation." Journal of Fluid Mechanics 360: 121-140.

Glezer, A. (1988). "The formation of vortex rings." Physics of fluids 31(12): 3532-3542.

Krueger, P. (2010). "Vortex ring velocity and minimum separation in an infinite train of vortex rings generated by a fully pulsed jet." Theoretical and Computational Fluid Dynamics 24(1): 291-297.

Krueger, P. and M. Gharib (2005). "Thrust augmentation and vortex ring evolution in fully pulsed jets." AIAA Journal 43(4): 792-801.

Kundu, P. K. and I. M. Cohen (2004). Fluid Mechanics, Elsevier Academic Press.

Lim, T. T. (1997). "A note on the leapfrogging between two coaxial vortex rings at low Reynolds Numbers." Physics of Fluids 9(1): 239-241.

Lim, T. T. and T. B. Nickels, (1995). Vortex Rings. In Fluid Vortices, Editor: Sheldon I. Green, Kluwer Academic Publisher.

Liu, G. C. and C. H. Hsu (1985). "Numerical studies of interacting vortices." NASA Technical Memorandum 86325.

Maxworthy, T. (1972). "The structure and stability of vortex rings." Journal of Fluid Mechanics 51: 15-32.

Maxworthy, T. (1977). "Experimental studies of vortex rings." Journal of Fluid Mechanics 81(03): 465-495.

Oshima, Y. and N. Izutsu (1988). "Cross-linking of two vortex rings." Physics of Fluids 31(9): 2401-2403.

Oshima, Y., T. Kambe, and S. Asaka (1975). "Interaction of two vortex rings moving along a common axis of symmetry." Journal of the Physical Society of Japan 38(4): 1159.

Raffel, M., C. E. Willert, S. T. Wereley, and J. Kompenhans, (2007). Particle Image Velocimetry, Springer.

Rayner, J. M. V. (1979) (a). "A vortex theory of animal flight. Part 1. The vortex wake of a hovering animal." Journal of Fluid Mechanics 91(04): 697-730.

Rayner, J. M. V. (1979) (b). "A vortex theory of animal flight. Part 2. The forward flight of birds." Journal of Fluid Mechanics 91(04): 731-763.

Shariff, K. and A. Leonard (1992). "Vortex rings." Annual Review of Fluid Mechanics 24(1): 235-279.

Weigand, A. and M. Gharib (1997). "On the evolution of laminar vortex rings." Experiments in Fluids 22(6): 447-457.

Yamada, H. and T. Matsui, (1978). "Preliminary study of mutual slip-through of a pair of vortices." Physics of Fluids 21: 292-294.